Geophysical Journal International

Geophys. J. Int. (2017) **210,** 1659–1680
Advance Access publication 2017 June 9
GJI Geodynamics and tectonics

doi: 10.1093/gji/ggx252

Flexural bending of the Zagros foreland basin

Mortaza Pirouz,[1,2] Jean-Philippe Avouac,[1] Adriano Gualandi,[1] Jamshid Hassanzadeh[1] and Pietro Sternai[3]

[1]*Division of Geological and Planetary Sciences, California Institute of Technology, Mc* 100–23, 1200 *E California Blvd., Pasadena, CA* 91125, *USA. E-mail: mpirouz@caltech.edu*
[2]*Bullard Laboratories, Madingley Rise, Madingley Road, University of Cambridge, Cambridge CB*3 0*EZ, United Kingdom*
[3]*Section of Earth and Environmental Sciences, University of Geneva,* 13 *Rue des Maraîchers,* 1205 *Geneva, Switzerland*

Accepted 2017 June 7. Received 2017 June 5; in original form 2017 February 24

SUMMARY

We constrain and model the geometry of the Zagros foreland to assess the equivalent elastic thickness of the northern edge of the Arabian plate and the loads that have originated due to the Arabia–Eurasia collision. The Oligo-Miocene Asmari formation, and its equivalents in Iraq and Syria, is used to estimate the post-collisional subsidence as they separate passive margin sediments from the younger foreland deposits. The depth to these formations is obtained by synthesizing a large database of well logs, seismic profiles and structural sections from the Mesopotamian basin and the Persian Gulf. The foreland depth varies along strike of the Zagros wedge between 1 and 6 km. The foreland is deepest beneath the Dezful embayment, in southwest Iran, and becomes shallower towards both ends. We investigate how the geometry of the foreland relates to the range topography loading based on simple flexural models. Deflection of the Arabian plate is modelled using point load distribution and convolution technique. The results show that the foreland depth is well predicted with a flexural model which assumes loading by the basin sedimentary fill, and thickened crust of the Zagros. The model also predicts a Moho depth consistent with Free-Air anomalies over the foreland and Zagros wedge. The equivalent elastic thickness of the flexed Arabian lithosphere is estimated to be *ca.* 50 km. We conclude that other sources of loading of the lithosphere, either related to the density variations (e.g. due to a possible lithospheric root) or dynamic origin (e.g. due to sublithospheric mantle flow or lithospheric buckling) have a negligible influence on the foreland geometry, Moho depth and topography of the Zagros. We calculate the shortening across the Zagros assuming conservation of crustal mass during deformation, trapping of all the sediments eroded from the range in the foreland, and an initial crustal thickness of 38 km. This calculation implies a minimum of 126 ± 18 km of crustal shortening due to ophiolite obduction and post-collisional shortening.

Key words: Numerical modelling, Continental margins: convergent; Crustal structure; Lithospheric flexure; Sedimentary basin processes.

1 INTRODUCTION

The Mesopotamian plain and the Persian Gulf form the peripheral foreland basin of the Zagros (Fig. 1). The basin developed during the late Cenozoic in response to the collision between Arabia and Eurasia as thrust sheets were transformed over the Arabian lithosphere (Snyder & Barazangi 1986; DeCelles & Giles 1996; DeCelles 2011). Recent studies of the basin filling history show that the Zagros flexure developed mainly over the last 20 Ma (Homke *et al.* 2004; Emami 2008; Khadivi *et al.* 2010; Pirouz *et al.* 2016), concurrently with crustal thickening and exhumation of the wedge (Gavillot *et al.* 2010; Khadivi *et al.* 2012; Mouthereau *et al.* 2012). The current view about the formation of foreland basins is that the basement is flexed down by overthrusting sheets in the wedge and sediment accumulation in the subsiding foredeep (Beaumont 1981; Karner & Watts 1983; DeCelles & Giles 1996; DeCelles 2011; Mouthereau *et al.* 2012). Static subsurface loads due to the density distribution at depth might also contribute to the force balance acting on the foreland deflection; for example, a subducted oceanic slab or a thickened lithospheric root. Dynamic stresses associated with mantle flow could also play a role (e.g. Karner & Watts 1983; Royden 1988, 1993; Garcia-Castellanos 2002). Therefore, the geometry and filling history of foreland basin hold clues about the dynamics of the associated orogeny and the ability of the lithosphere to support the topography and subsurface loads whether of static (due to hydrostatic buoyancy) or dynamic origin (due to stresses induced by mantle flow).

Gravity data offer a complementary source of information on subsurface loads and the mechanical support of the topography (e.g. Molnar and Lyon-Caen 1988; Watts 2001). Compared to the gravity

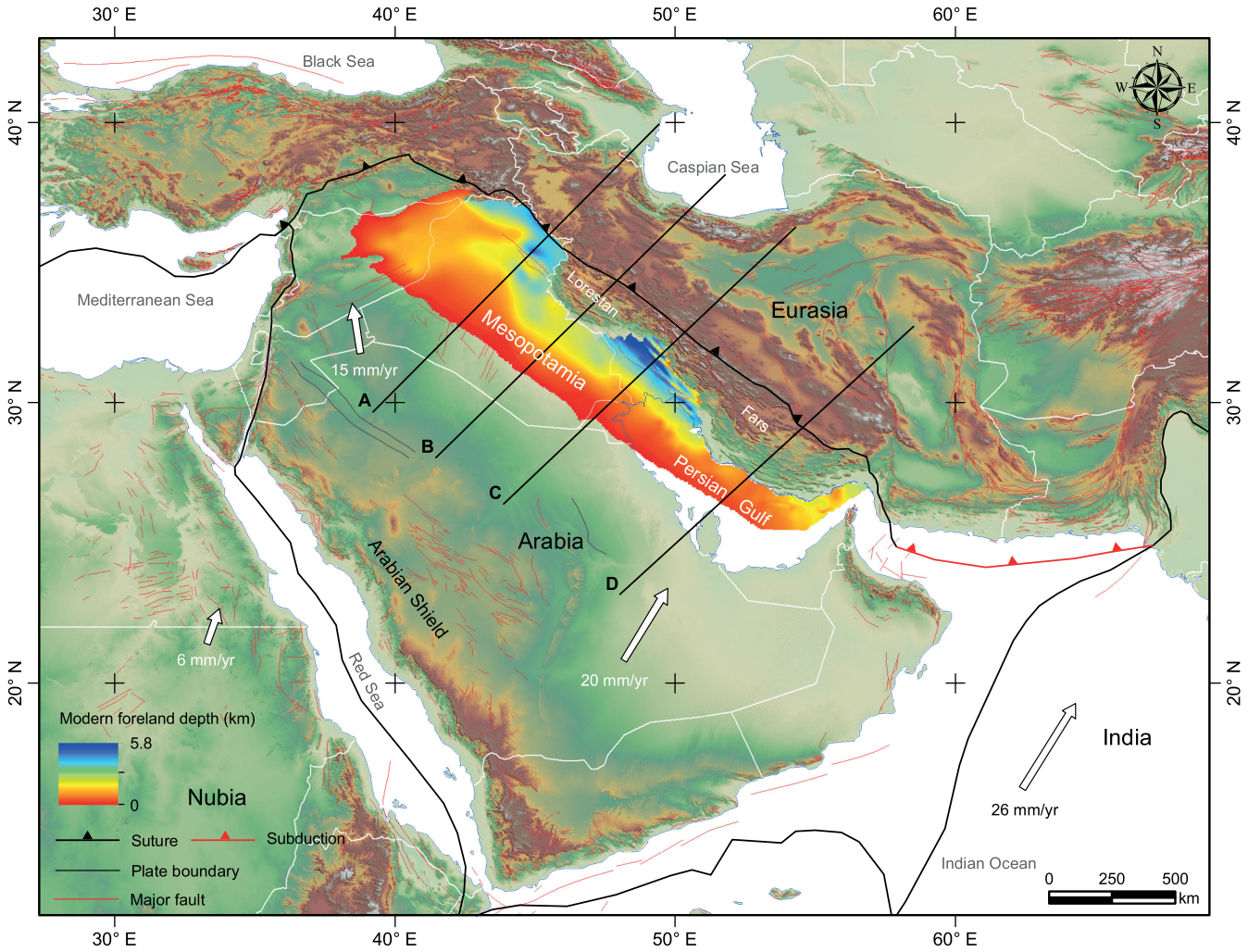

Figure 1. Plate tectonic setting of the Arabia–Eurasia collision zone. Depth to the Zagros foreland basin, defined as the top of the Asmari Formation, is determined in this study. White arrows represent plate motion relative to stable Eurasia (Reilinger & McClusky 2011).

signal that would be expected from a local isostatic compensation of the topography, the gravity measurements from the Zagros area indicate a deficit of mass on the foreland's side and an excess of mass on the wedge's side (Snyder and Barazangi 1986; Balmino *et al.* 2012; Bonvalot *et al.* 2012; Jimenez-Munt *et al.* 2012; Kaban *et al.* 2016). This pattern, which is expected in case of a flexural support of the range topography, was reported for the Zagros early on by Snyder & Barazangi (1986) who modelled the gravity data available at the time, and concluded that the topography of the Zagros seemed insufficient to explain the gravity anomalies. They therefore concluded that subsurface loads or dynamic stresses were needed in addition to the topographic load. More recently, Saura *et al.* (2015) modelled a section of the Zagros foreland and reached the conclusion that additional subcrustal load is necessary to account for the observed flexure.

From surface wave tomography, Priestley *et al.* (2012) imaged a thickened lithosphere that coincides clearly with the high topography and the thickened crust of the Zagros (Paul *et al.* 2010; Manaman *et al.* 2011; Fig. 2). Large variations of the lithospheric thickness are also suggested from the combined modelling of Bouguer anomalies and geoid height (Jimenez-Munt *et al.* 2012). This analysis has been augmented recently with additional constraints from body-wave tomographic results and petro-physical modelling (Tunini *et al.* 2015). These authors found evidence for important lateral variations of the composition of the lithospheric mantle suggesting variations of the buoyancy of the lithosphere. Static and dynamic stresses in relation to these variations and to subduction of the Arabian Lithosphere and slab break-off (Bird 1978) and the possible delamination of the thickened lithosphere (Hatzfeld & Molnar 2010) could have impacted the range topography and flexure of the foreland basin.

A related and debated topic regards the mechanical strength of the lithosphere. The support of the deficit of mass below the foreland and excess mass of the range topography requires that the continental lithosphere has some flexural rigidity, which is commonly quantified by the equivalent elastic thickness (e.g. Burov & Diament 1995), and could vary significantly based on its composition and thermal structure (Watts & Burov 2003; Jackson *et al.* 2008). The coherence between topography and gravimetry anomalies at the scale of the Arabian Peninsula suggests a rather large equivalent elastic thickness beneath the Zagros foreland of about 50 km (Chen *et al.* 2015). However, it has been suggested that the equivalent elastic thickness, T_e, derived from gravity data using such a spectral method could be overestimated in areas of low topography and that an admittance technique would be more reliable. It also avoids the possible bias introduced in case of correlated

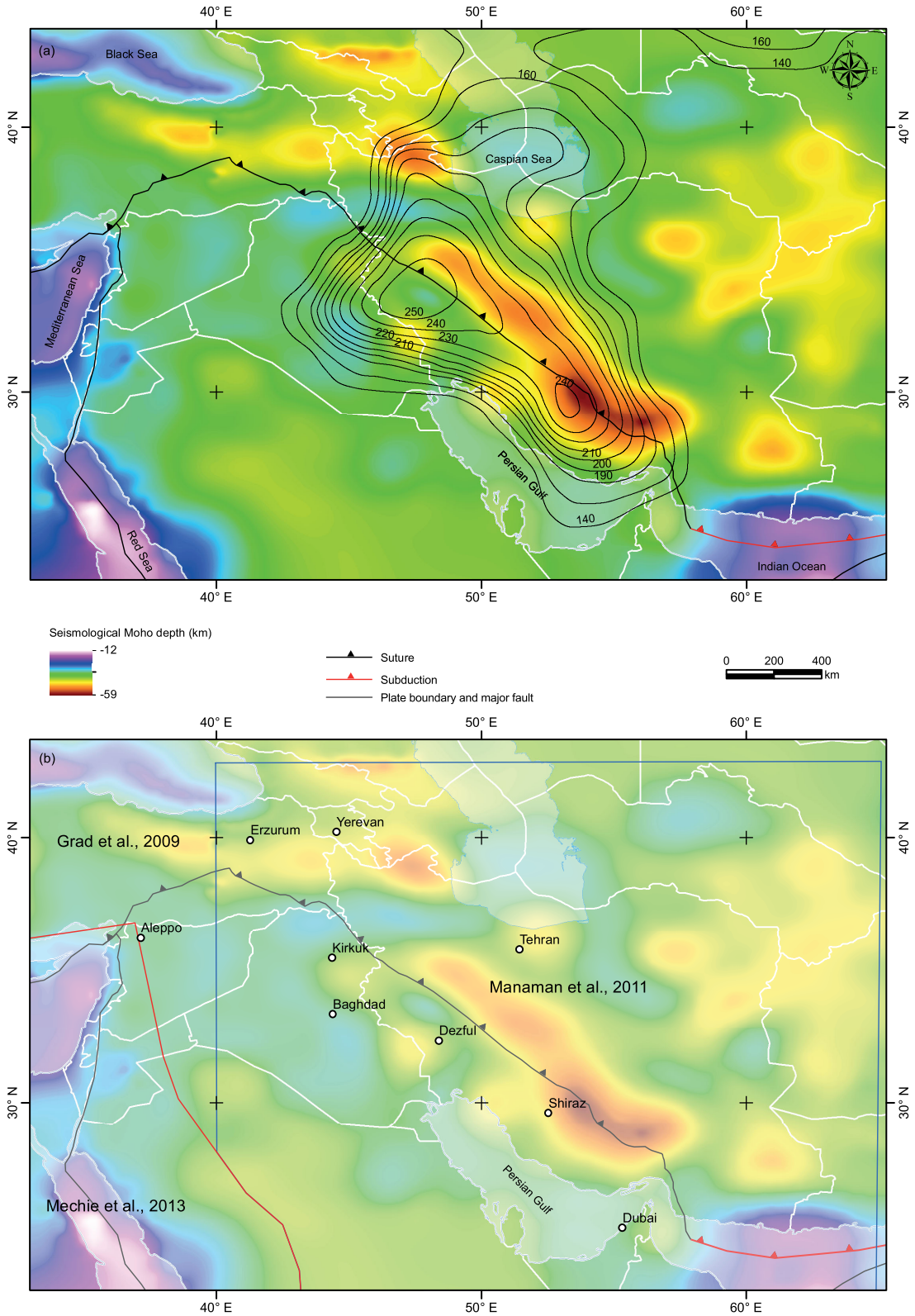

Figure 2. (a) Moho depth and lithospheric thickness. Black contour lines show depth to the lithosphere–asthenosphere boundary obtained from surface wave tomography (Priestley *et al.* 2012). Colour shading shows Moho depth obtained by combining results from regional body-wave seismological investigations by Grad *et al*. (2009), Manaman *et al*. (2011) and Mechie *et al*. (2013). The footprints of the various Moho models combined in panel (a) are shown in panel (b).

surface and subsurface loads (McKenzie & Fairhead 1997; McKenzie 2003). More recent studies have shown a methodological bias in this analysis, however if coherence and admittance techniques are applied with proper care, similar T_e values will be resulted (Pérez-Gussinyé *et al.* 2004; Pérez-Gussinyé & Watts 2005). Also, the correlation of surface and subsurface loads can in principle be identified in the complex coherency (Kirby & Swain 2009), but in that case the spectral approach cannot be used.

In this study we address how the geometry of the Zagros foreland basin relates to the loading by the range topography. To that effect we constrain the basin's geometry via available well logs, seismic profiles, structural sections and modelling. We also use gravity data to test the models predictions regarding the Moho's geometry. At first, we describe the large database that is used to constrain the basin geometry and density of sediments. Next, we describe our flexural model of the Arabian lithosphere loaded by crustal thickening and sediment load, which fits best to the observed geometry of the foreland as well as the gravity data. We resort to a simple model of thin elastic plate flexural bending which is a convenient representation of the continental lithosphere (Burov & Diament 1995). Then, we use the Moho depth predicted by the modelling to calculate crustal shortening assuming conservation of crustal mass.

2 GEOLOGICAL SETTING OF NORTHERN EDGE OF THE ARABIA

The northern margin of the Arabian plate underwent almost continuous marine sedimentation since the Cambrian (Stocklin 1968; Falcon 1974; Berberian & King 1981; Koop *et al.* 1982; Beydoun *et al.* 1992; Alavi 2004; Sepehr *et al.* 2006). This resulted in Palaeozoic epicontinental deposits, Permian-Triassic platform deposits, and Jurassic to middle Cretaceous continental shelf deposits. Subduction of the Arabian margin beneath the Eurasia continued until the Early Miocene leading to continent–continent collision during the Neogene (e.g. Alavi 2004; Agard *et al.* 2005). The entire sedimentary sequences overlying the crystalline basement has a thickness of 10–14 km in the Fars and Dezful regions in Iran which decreases to 6–10 km towards the south and northwest in Iraq and Syria. Thermochronology and structural studies indicate that crustal thickening and exhumation of the Zagros began around 30 ± 5 Ma marking the onset of the continent–continent collision between Arabia and Eurasia (Gavillot *et al.* 2010; Agard *et al.* 2011; Khadivi *et al.* 2012; Mouthereau *et al.* 2012). The Zagros foreland develops after the collision and displays a broadly upward-coarsening regressive megacycle that records the progressive uplift and southward migration of the Zagros wedge through time (Alavi 2004; Jassim & Goff 2006; Heydari 2008; Pirouz *et al.* 2015). The beginning of the foreland sequence is considered to coincide with the base of the Gachsaran Formation in Iran and Lower Fars in Iraq and Syria. This formation includes *ca.* 1 km of evaporitic deposits and variegated marl interbeds in Iran, which is thinner in Iraq and Syria, and has a clastic equivalent known as the Razak formation in the High Zagros and Fars areas (Motiei 1993; Pirouz *et al.* 2011). This formation separates the overlying foreland basin deposits from the older platform carbonates, i.e. the Asmari in Iran, the Euphrates-Jeribe in Iraq and the Chilou in Syria. For convenience, hereafter we use the term 'Asmari' to refer to these various platform carbonates formations.

Today, the Mesopotamian plain and the Persian Gulf form a single modern basin which extends over 2000 km in front of the Zagros wedge, a region spanning across southern Iran, Iraq and eastern Syria (Fig. 1). This basin is considered as an archetype example of a foreland which formed at the periphery of a collisional orogen (DeCelles & Giles 1996; DeCelles 2011). The basin is marine in the east where it coincides with the present day underfilled Persian Gulf with average water depth of 35 m and a maximum depth of 100 m at the Strait of Hormuz (Emery 1956; Purser & Seibold 1973), while it is overfilled and is non-marine in the west (Fig. 1). The Mesopotamian basin consists of an extensive, low relief flood plain occupied by several major meandering rivers, for example, Tigris and Euphrates to the northwest of the Persian Gulf. The sedimentary facies of the Neogene foreland basin deposits can be tracked to the surface and they remarkably match the modern sedimentary environments (Pirouz *et al.* 2011).

3 GEOMETRY OF THE ZAGROS FORELAND

In order to constrain the post-collisional subsidence in the Zagros foreland, we track the top of the Asmari carbonate platform limestone as the marker of the onset of foreland clastic sedimentation. We assembled a database using Petrel software (Fig. 3) that includes a large number of subsurface data, isopachs and geological maps (Brew *et al.* 1999; Alavi 2004; Abdollahie Fard *et al.* 2006; Jassim & Goff 2006; Sherkati *et al.* 2006; Jahani *et al.* 2009; Kent 2010; Soleimani 2010; Perotti *et al.* 2011; Pirouz 2013; Baban *et al.* 2014; Pirouz *et al.* 2014). The data set presented in this study is updated with seismic data (Sherkati *et al.* 2006; Jahani *et al.* 2009; Soleimani 2010; Perotti *et al.* 2011) and covers a larger area compared with previous compilations (Koop *et al.* 1982; Abdollahie Fard *et al.* 2006). The target surface, the top of the Asmari and its equivalents, was digitized and then interpolated in order to obtain a surface representing geometry and depth of the foreland basin. Geological maps published by Iranian National Oil Company were used, mostly in the eastern sector, Dezful embayment, to track the structural axes. Data for Iraq are limited to isopach maps and few interpreted seismic lines (Jassim & Goff 2006), while available data for Syria include a good coverage of seismic lines and boreholes. We used the interpreted Neogene horizon by Brew *et al.* (1999) for Syria in our compilation. The contact between Asmari massive limestone and Neogene foreland deposits can be easily distinguished in the seismic data (Abdollahie Fard *et al.* 2006; Jahani *et al.* 2009; Soleimani 2010; Perotti *et al.* 2011) and is controlled by large number of the boreholes. The geometry of the foreland can thus be constrained over the extent of the entire modern Zagros basin (Figs 1 and 4). The result shows a deep and narrow foredeep in the Dezful embayment where the maximum depth of the foreland occurs at a depth of *ca.* 6 km, whereas it is shallower and wider towards both ends. An average depth of the basin is *ca.* 3.5 km in Iraq, *ca.* 0.5–1.5 km in Syria in the western sector and less than several hundred meters in the Persian Gulf just in front of the Fars region but gets slightly deeper towards the Strait of Hormuz in the east with respect to the present-day sea level. Post-Asmari folding and thrusting is obvious in the seismic sections near the Zagros deformation front, in particular within the Dezful embayment (Sherkati *et al.* 2006). This observation suggests two possibilities (Verges *et al.* 2011): (1) the passive margin sedimentary cover is deformed due to a main detachment level within the sedimentary or at the base of the sedimentary cover, (2) both sedimentary cover and basement are deformed. The second interpretation is more likely as basement deformation has been inferred from seismological observations (Jackson 1980; Talebian & Jackson 2004), and basement

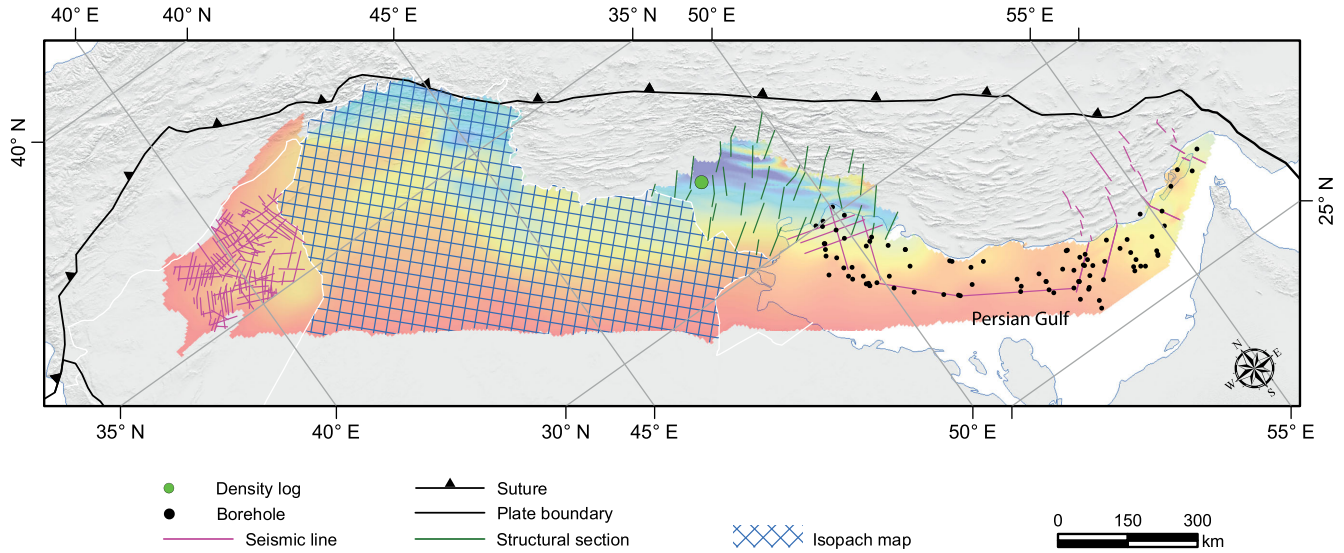

Figure 3. Locations of the 2-D seismic lines and structural sections (interpreted from seismic lines), borehole data and iso-depth maps used to reconstruct depth to the top of the Asmari Formation and its equivalent in the northern margin of the Arabian plate. Data sources: (Brew *et al.* 1999; Alavi 2004; Abdollahie Fard *et al.* 2006; Jassim & Goff 2006; Sherkati *et al.* 2006; Jahani *et al.* 2009; Kent 2010; Soleimani 2010; Perotti *et al.* 2011; Pirouz 2013; Baban *et al.* 2014; Pirouz *et al.* 2014). Green circle shows approximate location of the well data used to estimate depth variation of density of the sedimentary fill.

deformation is in fact visible in some seismic profiles in the eastern corner of the Dezful embayment (Sherkati *et al.* 2006). Southwards of this deformation zone, the Asmari formation is less deformed and shows a gradual flexure qualitatively consistent with the flexure of a bent elastic plate. Our compilation yields a model of the foreland geometry at the regional scale. Comparison with local estimates form previous studies show only minor differences generally of the order of a few hundred meters. The largest mismatch is observed in the deepest part of the basin in Dezful embayment where Abdollahie Fard *et al.* (2006) estimated a depth larger than 6 km and Koop *et al.* (1982) assessed a depth of 5.5 km, whereas our model shows a depth of 5.8 km.

4 SOURCE OF LOADS, DENSITY MODEL AND SEISMOLOGICAL MOHO CONSTRAINTS

As the orogen grows, topography and its subsurface root develop, thus the topography represents only a fraction of the vertical load source flexing down the lithosphere. In addition, the weight of basin deposits and the water bodies further contribute to produce vertical forces bending the incoming plate (Beaumont 1981; Watts 2001). The role of sedimentary load is particularly important in the case of the Zagros, where the volume of the post-collisional deposits is comparable to the topography of the range above sea-level (Figs 4 and 7).

Current topographic load can be estimated easily using a digital elevation model. We use the topographic SRTM model (Farr *et al.* 2007), and the standard density for the upper crust ($\rho_c = 2670$ kg m^{-3}) of the WGM2012 global density map. The restoring force due to buoyancy of the crustal root defined by the deflection of the Moho needs also to be taken into account. We assume that the Moho is the only significant density discontinuity in the subsurface and that it is deformed conformably with lithospheric bending. The restoring force depends on the density contrast between Moho and the material filling in the depression of the lithosphere at the surface, $\Delta\rho = \rho_m - \rho_{infill}$.

We determined a local value of the density increase at Moho, $\Delta\rho$, and the reference crustal thickness for a crust with zero topography and in isostatic balance, T_c, using the free-air anomaly (FAA) and seismological constraints on the Moho depth. We used the World Gravity Map (WGM12), which is the latest high-resolution global grid of the Earth gravity field of the Bureau Gravimétrique international (Bonvalot *et al.* 2012). WGM 2012 was derived from space, airborne and terrestrial measurements and includes a $1' \times 1'$ resolution terrain correction computed based on the global relief model, ETOPO1, considering the contribution of the various sources of surface masses (atmosphere, land, oceans, inland seas, lakes, ice caps and ice shelves).

We estimate the theoretical gravity signal assuming the density contrast at the Moho to be the only subsurface source of gravity anomaly in addition to the effect of the sedimentary fill of the basin (see details in the Supporting Information). We estimate the density variation with depth in the Zagros basin using data from a well located in the Dezful embayment (green circle in Figs 3 and 4). These data indicate that the density increases from *ca.* 1.9 g cm^{-3} near the surface to a reach standard crustal density of *ca.* 2.6 g cm^{-3} at a depth of 4 km.

The Moho depth (Fig. 2) is based on a compilation of seismological models for the Iranian, Arabian and European plates (Grad *et al.* 2009; Manaman *et al.* 2011; Mechie *et al.* 2013; Fig. 2). The Moho depth for the Zagros and its foreland is mostly based on Manaman *et al.* (2011). The best fitting values of $\Delta\rho$ and T_c depend on the geographical area selected for the inversion. This finding is consistent with Kaban *et al.* (2016) who used the seismological Moho depth model of (Stolk *et al.* 2013) and produced a regional map of the lateral variations of the mantle density needed to reconcile the Moho depth model with the gravity anomaly map. Here, we are interested in a more restricted area (Fig. 4) within which lateral variations of mantle density are probably less severe than at the scale of the whole Arabian Peninsula considered by Kaban *et al.* (2016). Our Fig. 5 shows the theoretical FAA calculated from the compiled seismic Moho depth for the best fitting values of $T_c = 37.8$ km and $\Delta\rho = 390$ kg m^{-3}. These values yield a root-mean-square error

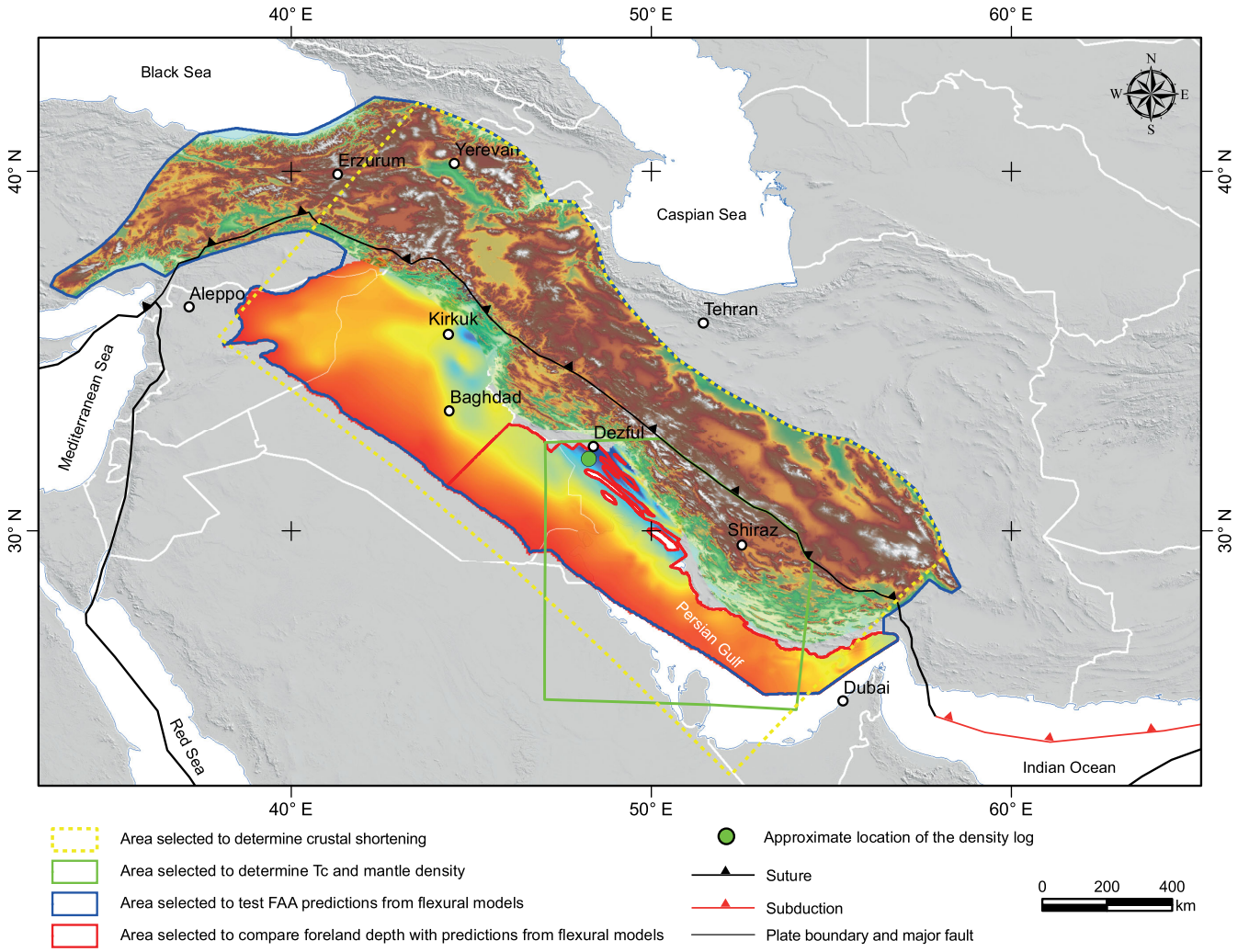

Figure 4. Post-collisional foreland basin depth and the Zagros wedge topography used in our flexural bending calculations. We outline three different areas that were used to compare the model predictions with the observations. The area outlined with blue is used to compare the observed free-air anomalies (FAAs) with predicted FAAs by our flexural models. The area outlined with yellow dash-line is used to estimate crustal shortening from a mass balance budget. The area outlined with green is used to compare observed FAA with the predicted FAA obtained from the seismic Moho determined by Manaman *et al.* (2011) and adjust the density contrast at the Moho to best reconcile the seismological observations with the observed FAA. The area outlined with red is used to compare the foreland depth determined from the Asmari with the depth predicted by our flexural models. The area where the Asmari has been folded and thrusted is cropped out. Green circle shows approximate location of the well data used to estimate depth variation of density of the sedimentary fill.

(RMSE) of 73 mGal (Supporting Information Fig. S1). The predicted FAA resembles the observed FAA to first order only. It does not reproduce well in particular the pair of positive and negative anomalies, respectively in the range and basin, which is expected from flexural support of the topography, while it is detected in the observed FAA (Fig. 5a). Flexural support would indeed imply the Moho to be deeper than predicted from local isostasy beneath the foreland, and hence a negative uncompensated topography (Fig. 5c). Beneath the range we would expect a positive uncompensated topography, that is, a Moho depth shallower than predicted from local compensation of the topography. Comparison of the Moho depth derived from seismology with the Moho depth predicted from local isostasy along profiles (Fig. 6) shows that flexural effects are not as obvious as in the gravity signal and foreland geometry. We also note that the seismological Moho of Manaman *et al.* (2011) is not parallel to the geometry of the foreland base as would be expected in case of flexural bending of the lithosphere. We also tested the Moho model of Stolk *et al.* (2013) and found similar issues (Fig. 6). Inconsistencies between the measured FAA and the FAA predicted from the seismological constraints are possibly due to errors in the interpretation of the seismological data, errors introduced by the interpolation technique used to build the 2-D model from the initial data set, and finally lateral variations of crustal and mantle densities which are ignored in the calculation of the predicted FAA. To insure consistency with observed flexure of the foreland and FAA, we determine a model of the Moho geometry assuming that it was initially flat and deformed as predicted by our flexural model. In the following calculations, we use rounded values of $\Delta\rho = 400\ \mathrm{kg\,m^{-3}}$ and $T_c = 38\ \mathrm{km}$ to ensure consistency with the seismic Moho on average. We also present flexural models calculated with $\Delta\rho = 300$, 350, 450 and 500 $\mathrm{kg\,m^{-3}}$.

5 FLEXURAL BENDING MODEL

Flexure of the Arabian plate is calculated assuming an elastic thin plate over an inviscid fluid. We take the weight of the range

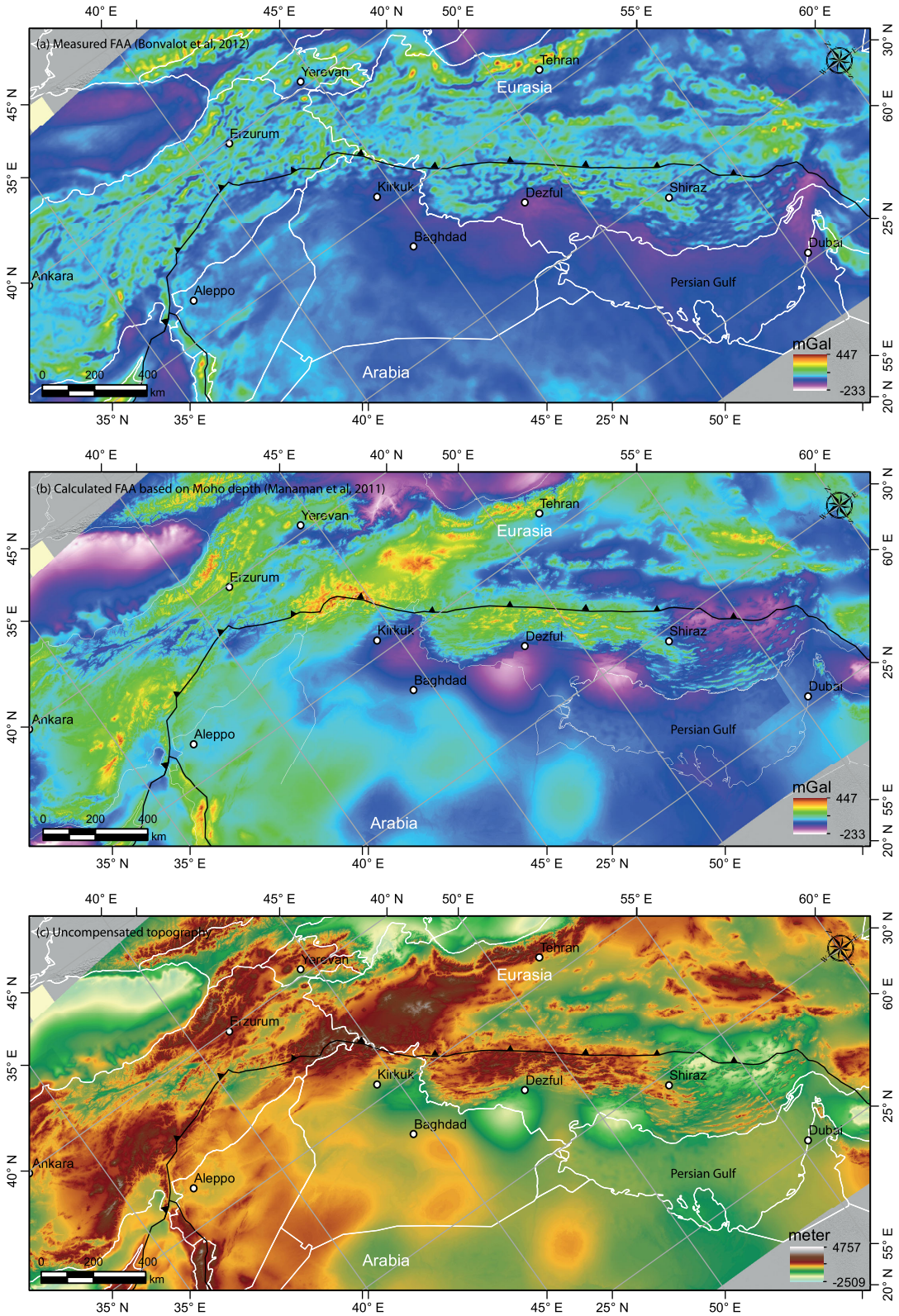

Figure 5. (a) Measured free-air anomaly (FAA) at the surface (Bonvalot *et al.* 2012). (b) Predicted FAA using the seismological Moho of Manaman *et al.* (2011) and taking into account the post-Asmari foreland sediments (see the Supporting Information for details). The best fit is obtained for $T_c = 37.8$ km and $\Delta\rho = \rho_m - \rho_c = 390$ kg m^{-3}. (c) Uncompensated topography calculated from the difference between the observed topography and the topography predicted for local isostasy. We assume an Airy compensation scheme with density contrast only at the surface and at the Moho with $T_c = 37.8$ km, $\Delta\rho = \rho_m - \rho_c = 400$ kg m^{-3} and $\rho_c = 2670$ kg m^{-3}.

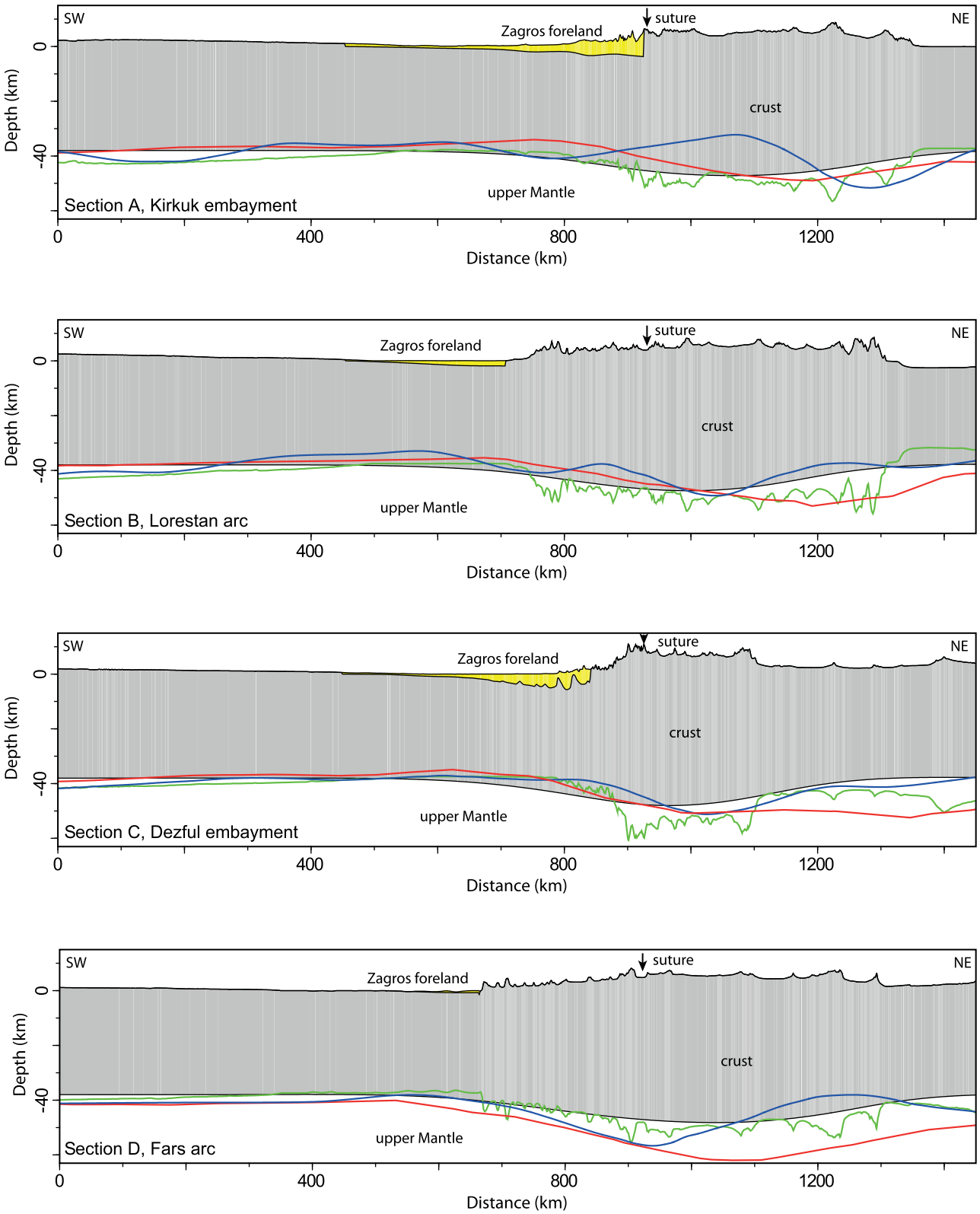

Figure 6. Crustal cross-sections. See Fig. 1 for location of profiles. Topography is exaggerated (3x). We show the Moho depths derived from seismological constraints by Manaman *et al*. (2011) in blue, and by Stolk *et al*. (2013) in red. The green line is the Moho predicted from local compensation of the topography. We used $T_c = 38$ km and $\Delta\rho = \rho_m - \rho_c = 400$ kg m^{-3} as determined from least-squares fitting of the FAA using the seismological Moho of Manaman *et al*. (2011) and taking into account the post-Asmari foreland sediments; see the Supporting Information for details. The Moho depth resulted from our preferred model (Model 2) is used to separate the crust (grey) from the upper mantle (white). The equation to calculate crustal Airy root is: $R_{(x,y)} = -[T_c + (\frac{\rho_c \times H_t}{\rho_m - \rho_c})]$ where $R_{(x,y)}$ is Airy root, T_c is non-deformed crust at isostatic equilibrium, H_t is topography, ρ_m is the mantle density, and ρ_c is the crust density.

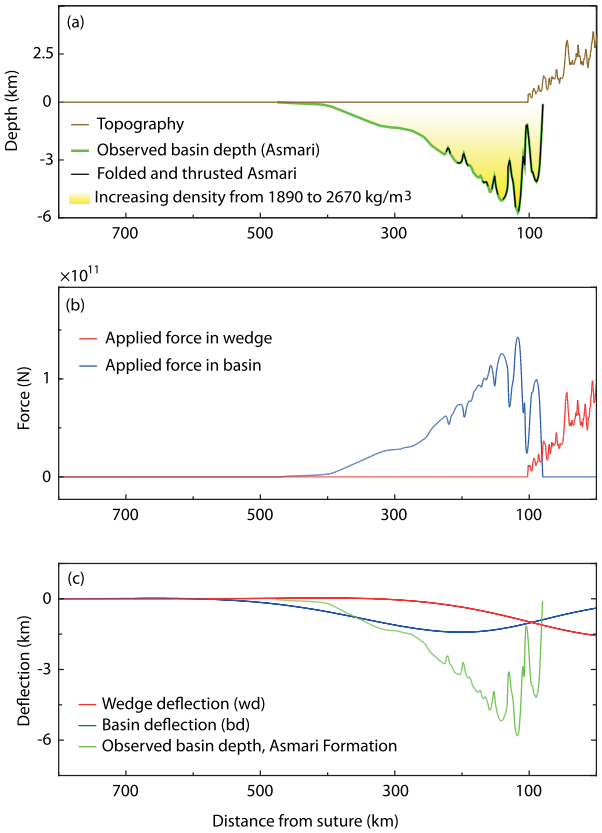

Figure 7. (a) Topography (Brown line) and depth to the Asmari formation (green line) along section C which runs across the Dezful embayment (Fig. 1). Portions highlighted in black correspond to areas where the Asmari is clearly affected by thrusting and folding. These areas are not considered to find best fit between predictions of flexural bending of a thin elastic plate and observed deflection represented by the Asmari Formation. (b) Surface distribution of load due to the sediment weight (blue) and topography (red). (c) Deflection of an elastic thin plate with equivalent elastic thickness of $T_e = 50$ km due to the sediment weight (blue) and topography (red). Here the effect of the crustal root below the topography is not shown.

topography and basin fill as distributed sources of loads. We run the calculations using a convolution technique and the Green's functions of Brotchie & Silvester (1969) and Wienecke *et al.* (2007), derived from a 2-D analytical solutions of the fourth-order differential equation governing the deflection w. Although we found little differences between the two solutions, we use the approach of Wienecke *et al.* (2007) in this study. The Green's functions are truncated at a distance equal to 6 times the flexural parameter (β) (see the Supporting Information for details). This approach allows a better spatial resolution than the more commonly used spectral method and was therefore preferred in this study. Wienecke *et al.* (2007) have shown the consistency of the convolution approach with the spectral method (see their fig. 1). In this model of flexural support, the plate is assumed to have homogeneous properties. Lateral variations of equivalent elastic thickness, T_e, which may well exist at the scale of our study (Zamani *et al.* 2014; Chen *et al.* 2015) are thus ignored. In-plane stresses are ignored (no buckling) and non-hydrostatic basal tractions are neglected, as well as stresses due to dynamics below the lithosphere are ignored. Distribution of load is computed by taking into account the basin geometry and depth-distribution of density in the basin based on a density log from the Dezful embayment (Fig. 3 and Supporting Information Fig. S2). In such case the Green functions are calculated for a thin plate separating two media with the density of air ($\rho_a = 1.2$ kg m^{-3}) and mantle ($\rho_m = 3070$ kg m^{-3}). Supporting Information Fig. S3 shows the predicted signal for different values of the equivalent elastic thickness of $T_e = 5$, 20 and 50 km. The distribution of surface load along section C (Fig. 1) which runs through the Dezful embayment, where the post-Asmari subsidence is maximum, is shown in Fig. 7. This figure also shows the deflection calculated only due to the topographic load of the Zagros wedge, the weight of terrains with elevation above sea-level, for a relatively large elastic thickness value of $T_e = 50$ km (red line in Fig. 7c). This calculation assumes that the depressed topography of the foreland is replaced with air. Note that loading by the topography (above sea level) cannot explain the wavelength of the flexed foreland (red line in Fig. 7c). Fitting the observed wavelength would require an unrealistically large value of T_e. Loading by the sedimentary fill is thus clearly the primary factor controlling the width of the foredeep (blue line in Fig. 7c). Finally the calculation shows that the effect of the crustal root needs to be taken into account to explain the observed amplitude of the deflection.

5.1 Model 1: Topography, basin and crustal root equal to lithospheric deflection

In this model we apply topographic and basin loads and use the common assumption that the space created due to the Moho deflection is filled with material of crustal density. This model thus includes the static subsurface load associated to the buoyancy of

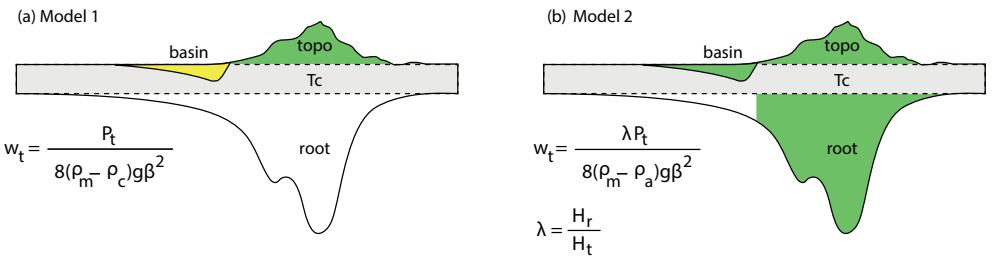

Figure 8. Schematic representation of Models 1 (a) and 2 (b). In Model 1 (a), the applied load is due to topography, and $\Delta\rho = (\rho_m - \rho_c)$. Assumption for calculation of the Green function stems from the fact that the space created by deflection of the Moho is filled with crustal density material. In that case the basin load in negative (yellow colour) as the deflection of the foreland leads to replacing mantle density material with sediment. In Model 2 (b), the applied load is calculated from the excess thickness of the crust compared to its initial thickness (T_c), and the Green function assumes that the space created by the deflection of the Moho is filled with air. Over the range, the load is calculated from the topography, the crustal root, and $\Delta\rho = (\rho_m - \rho_a)$. Over the basin, the load is positive (green colour) and is calculated from the weight of the sedimentary fill. Abbreviations are: T_c, thickness of undeformed lithosphere; w_t, maximum deflection due to topographic load; P_t, topographic load; ρ_m, density of Mantle; ρ_c, density of crust; ρ_a, density of air; g, gravity acceleration; β, flexural parameter; H_r, root thickness; H_t, topographic height.

the crustal root. This effect is incorporated in the calculation of the Green function which assumes that the deflection leads to replace material of mantle density, ρ_m, with crustal density material $\rho_c = 2670$ kg m^{-3} (instead of air as in the calculation of Fig. 7). A density contrast of $\Delta\rho = \rho_m - \rho_c = 400$ kg m^{-3} is assumed in the plotted in Figs 8–10. The results for $\Delta\rho = 300$ to 500 kg m^{-3} are reported in Table 1.

We calculated a range of models by varying the value of T_e between 1 and 100 km, which is the only adjustable parameter of this model, to minimize the root-mean-square error between the observed and predicted post-collisional deflection. To avoid a possible bias introduced by folding and thrusting of the Asmari formation near to the Zagros deformation front we cropped out areas corresponding clearly to such deformation (shown in Figs 4 and 7). For $\Delta\rho = 400$ kg m^{-3}, the best fitting model is obtained for $T_e = 54$ km (Fig. 9a) and yields an RMSE of 695 m (for the other values of $\Delta\rho$, see Table 1). The model produces a foreland deflection with a wavelength and amplitude comparable to the observed geometry of the foreland (Figs 10b and 11). However some systematic misfits are observed. The deflection is too small at distances larger than *ca.* 400 km, except in the Fars area (Fig. 10a and b).

We also tested the merit of such a model in explaining the FAA. We assume that the Moho is deformed conformably with the bent lithosphere. We thus determine the Moho depth by adding $T_c = 38$ km to the calculated deflection. FAA maps are obtained assuming $\rho_c = 2670$ kg m^{-3} and $\rho_m = 2970$–3170 kg m^{-3} (i.e. $\Delta\rho = 300$–500 kg m^{-3}) and compared to the observed FAA. For $\Delta\rho = 400$ kg m^{-3}, the best fitting model has an equivalent elastic thickness of $T_e = 53$ km remarkably close to that derived from the foreland subsidence (Fig. 9b). We note that the model fits the details of observed FAA much better than the Moho models derived from seismology (Figs 12 and 13, Supporting Information Figs S4 and S5). The RMSE is *ca.* 32 mGal (Fig. 9b). The observed positive and negative FAA anomalies over the Zagros wedge and basin are in particular reproduced well by this model. One drawback of this modelling approach is that the predicted deflection does not match the geometry of the foreland basin very well (see red lines in Fig. 11). The mismatch can be interpreted to suggest that a different loads distribution, and/or additional subsurface loading is necessary. Since the Green function assumes that the displaced mantle due to the Moho deflection is replaced with crust, and not sediments as would happen if the crust is bent elastically, the model is not internally consistent if the basin geometry is not correctly adjusted by the model.

5.2 Model 2: Topography, basin load and adjustable subsurface load correlated with topography

Here the deflection of the Moho is calculated taking topographic and basin loads into account and a simple parametrized representation of subsurface loads. We assume that the deflection is filled with air $\rho_a = 1.2$ kg m^{-3} and the subsurface load is proportional to the topographic load (Fig. 8b). The load from topography and subsurface loads is then simply λ times the topographic load. This approach allows to account for all subsurface loads correlated with topography, including the effect of the crustal root. Additional loads, potentially correlated with topography, could be due to inhomogeneities of crustal density, possibly due to the thermal structure of the range and metamorphic reactions associated with underthrusting and exhumation of Arabian crust. It could also account for the possible effect of the lithospheric core imaged by Priestley *et al.* (2012)

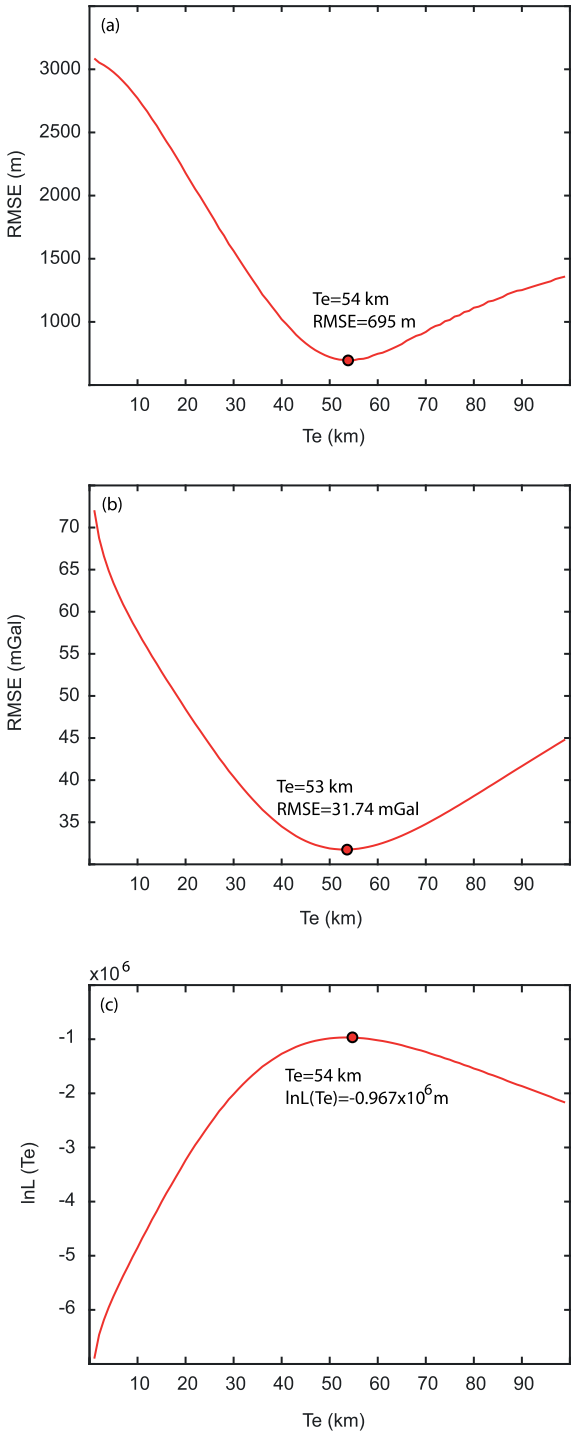

Figure 9. (a) Root mean-square error (RMSE) between observed and predicted foreland depths as a function of the equivalent elastic thickness, T_e, for the Model. (b) RMSE between observed and predicted free air anomalies (FAAs) over the Zagros foreland and wedge as a function of the equivalent elastic thickness, T_e, for the Model. (c) Logarithm of the likelihood (L) of the joint pdf that takes into account both of the deflection and FAA data sets. It is calculated as the sum of the squared RMSE of two data sets, weighted by a factor $-\frac{N_i}{2\delta_i^2}$. N_i is the number of data belonging to the ith data set, and δ_i^2 is the variance associated with the measurements of the ith data set. Such variance is estimated assuming the best fitting model to the ith data set has a reduced χ^2 equal to 1.

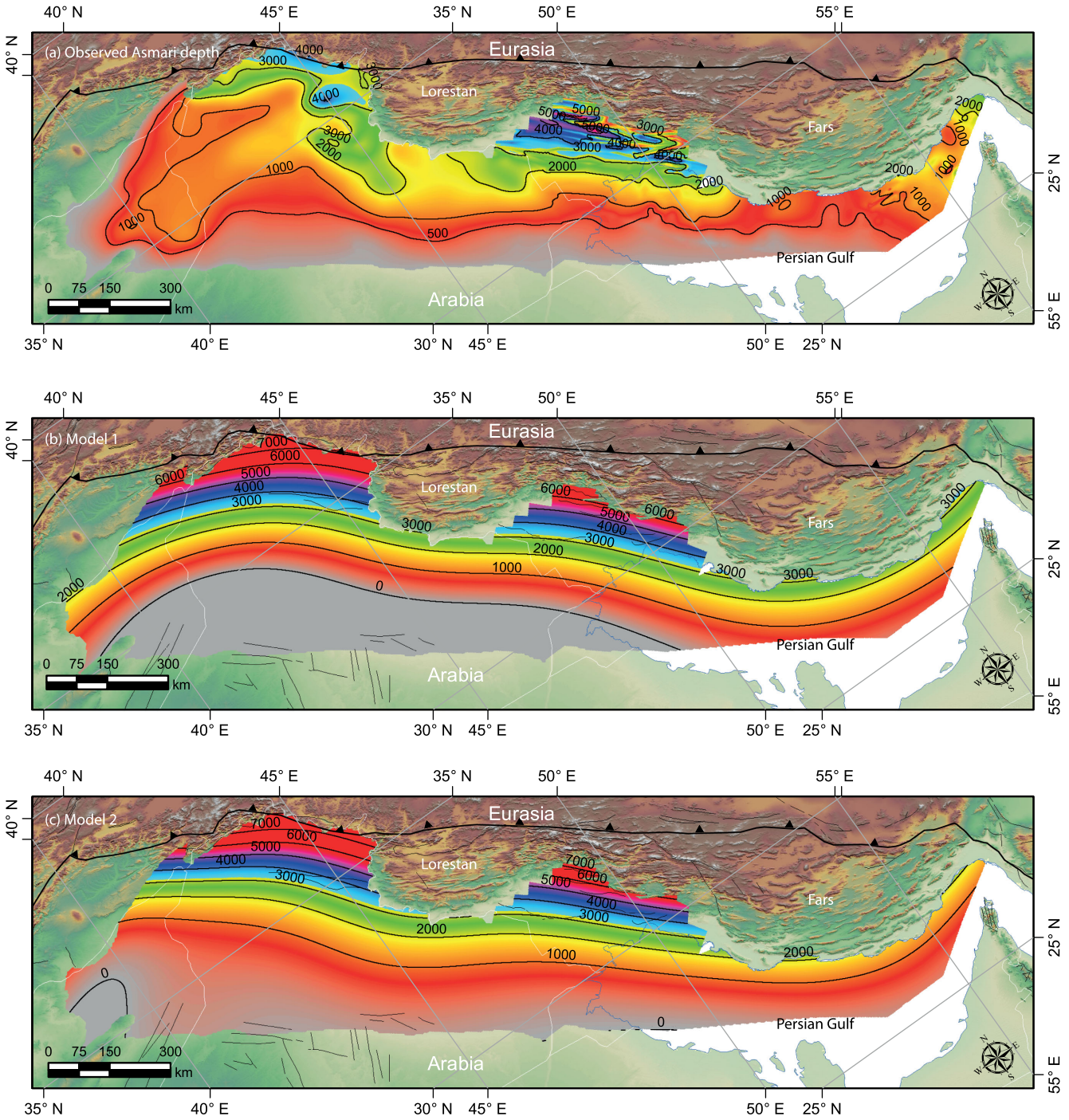

Figure 10. Observed (a) and predicted depth of the post-collisional foreland for best fitting Model 1 (b) and Model 2 (c). The area that was used in the calculation of the root mean-square error (RMSE) is shown as a red polygon in Fig. 4.

which coincides approximately with the Zagros topography. Such a core could generate static and kinematic stresses affecting the deflection of the lithosphere beneath the Zagros wedge and the adjacent foreland.

Model 2 depends thus on two adjustable parameters T_e and λ. We run different models with $T_e = 1$–100 km with step of 1 km and $\lambda = 0.1$–10 with step of 0.1 and determined the best fitting values from least squares fit to the foreland basin geometry (Fig. 14a) and FAA (Fig. 14b). For $\Delta\rho = 400$ kg m^{-3}, the inversion of the foreland geometry yields an equivalent elastic thickness $T_e = 59$ km and $\lambda = 5.1$ (see Table 1 for other values of $\Delta\rho$). The fit to the basin geometry drops to 327 m in Model 2 (Fig. 14a), and is much better than that obtained from Model 1. The f-test shows that the improved misfit is significant at the 99 per cent confidence level. The loads resulting from the basin fill and hydrostatic restoring force due to the Moho deflection are thus better represented in Model 2.

The inversion of the FAA over the Zagros and its foreland yields almost similar value for λ (Fig. 14b). For each single calculation, the value of T_e is less well constrained from the gravity data alone due to the trade-off between λ and T_e. For example, inversion of the FAA allows λ values between 5 and 6 for T_e values between 10 and 70 km (Fig. 14b, black zone). The value of T_e is thus less

Table 1. Summary of modelling results for Model 1 (one parameter: T_e) and Model 2 (two parameters: T_e, λ). Best fitting parameters and RMSE are listed for all models tested for different values of $\Delta\rho$. We also list the average shortening across the Zagros estimated from mass conservation assuming an initial crustal thickness $T_c = 38$ km.

Models	Density variation $\Delta\rho$ (kg m^{-3})	FAA			Deflection			Joint probability		Average shortening (km)
		T_e (km)	λ	RMSE (mGal)	T_e (km)	λ	RMSE (m)	T_e (km)	λ	
Model 1	300	48	–	31.75	44	–	1009.4	46	–	160.8
	350	51	–	31.75	49	–	821.2	50	–	139.8
	400	53	–	31.74	54	–	695.0	54	–	128.0
	450	55	–	31.75	59	–	625.3	57	–	112.1
	500	57	–	31.90	64	–	586.5	60	–	103.2
Model 2	300	32	7.3	30.03	56	4.9	319.1	38	7.3	153.4
	350	35	6.4	30.05	59	5.0	325.3	45	6.6	136.6
	400	31	5.6	30.06	59	5.1	326.9	50	5.9	125.8
	450	32	5.1	30.10	61	5.2	334.1	54	5.4	111.7
	500	29	4.6	30.16	61	5.3	329.7	60	5.1	104.5

well constrained with Model 2 than with Model 1. If the fits to the foreland geometry and FAA are combined after normalisation of the weight assigned to each data set (see the Supporting Information for details), we get that $T_e = 50$ km and $\lambda = 5.9$ yield the best possible fit to both data sets jointly (Fig. 14c). We show the case of $\Delta\rho = 400$ kg m^{-3} in Figs 10–13 where $T_e = 50$ km and $\lambda = 5.9$, while other cases are reported in Table 1.

6 DISCUSSION

6.1 Implications for the rheological layering of the continental lithosphere

The foreland basin geometry and the gravity anomalies over the Zagros and its foreland show evidence for flexural support; and these signals are reproduced to first order assuming a continuous plate with an equivalent elastic thickness of $T_e = 50 \pm 10$ km. The uncertainty associated to this estimate should be considered with caution as it accounts only for the sensitivity of the model predictions to T_e. The uncertainty on the Green's function, which depends in particular on the uncertainty on $\Delta\rho$, is also important as this quantity is not very well constrained and may vary spatially. We therefore assessed the range of possible value of T_e by running various inversions with different values of $\Delta\rho$ (listed in Table 1). By varying the density contrast at the Moho between 300 and 500 kg m^{-3}, the equivalent elastic thickness, T_e, varies from 38 to 60 km (Table 1). We therefore estimate the range of possible values required to fit jointly the foreland depth and FAA to between 38 and 60 km. This range of values is consistent with the equivalent elastic thickness of the lithosphere determined in previous studies based on the analysis of 1-D profiles in the eastern sector of our study area (about 50 km, Snyder & Barazangi 1986; Saura *et al.* 2015). It is also consistent with the equivalent elastic thickness mapped from the coherence between the topography and the gravity field (Chen *et al.* 2015), which shows a gradient from about 90 km for the Arabian Platform south of the Mesopotamia basin to about 30 km beneath the Zagros.

The *ca.* 38–60 km equivalent elastic thickness of the lithosphere of Arabian Platform, the age of which is estimated between 600 and 900 Ma (e.g. Stern & Manton 1987; Hargrove *et al.* 2006), is in the ballpark of values found for other continental areas with similar Neoproterozoic age (Burov 2011; Tesauro *et al.* 2013). This range of values informs us about the rheology of the continental lithosphere and, in particular, about the mechanical coupling between the crust and mantle, which controls where the strength of the continental lithosphere resides (Burov & Diament 1992; Watts & Burov 2003; Burgmann & Dresen 2008). The rather large values obtained in this study are consistent with mechanical coupling between the crust and upper mantle as suggested by previous models that account for depth variations of the continental rheology due to temperature and composition (Tesauro *et al.* 2012). A strong lower crust beneath the foreland basin would be consistent with the observation of deep earthquakes in the basement as much as 35 km (Jackson 1980; Jackson *et al.* 2008; Nissen *et al.* 2011). It thus seems that neither the 'crème-brûlée' model of the continental crust nor the 'Jelly sandwich' model are relevant; because as on the one hand, a strong coupling between the crust and mantle and some strength in the upper mantle are needed, and, on the other hand, T_e exceeds the crustal thickness, which requires adequate strength in the upper mantle. For comparison, the elastic thickness of the lithosphere beneath foreland basin of the Himalaya, which is of Proterozoic to Archean lithospheric age, is estimated to 60–80 km (Lyon-Caen & Molnar 1983; Cattin *et al.* 2001; Hetenyi *et al.* 2006; Mooney 2010). The modelling of the gravity data suggests that the equivalent elastic thickness beneath the Zagros range is probably significantly lower than beneath the foreland (we get a best fitting value of *ca.* $T_e = 30$ km when only the gravity data are used). Similarly low values of T_e have also been inferred there based on the coherence between topography and gravity anomalies over the range (Zamani *et al.* 2014; Chen *et al.* 2015). A northward gradual decrease in T_e is expected because of the bending-induced reduction of the elastic cores, and the presumably higher crustal temperatures within the range resulted from crustal thickening and vertical heat advection (e.g. Burov & Diament 1995; Cattin *et al.* 2001; Hetenyi *et al.* 2007).

6.2 Signature of sublithospheric dynamics

We find that the geometry of the foreland and Moho can be reasonably well explained with a simple model of an elastic plate flexed by static loads related to the topography and basin infill. Model 2 yields a significantly better fit to the observations than Model 1 (Table 1). It is not clear whether the improvement is due primarily to a better representation of the loads applied to the foreland basin (due to the sediment fill and hydrostatic buoyancy force associated to the Moho deflection) or because of a better representation of the loads applied on the range side. We now calculate the load due to crustal thickening implied by this model. We calculate the crustal thickness predicted by the model (crustal root+ topography above sea level)

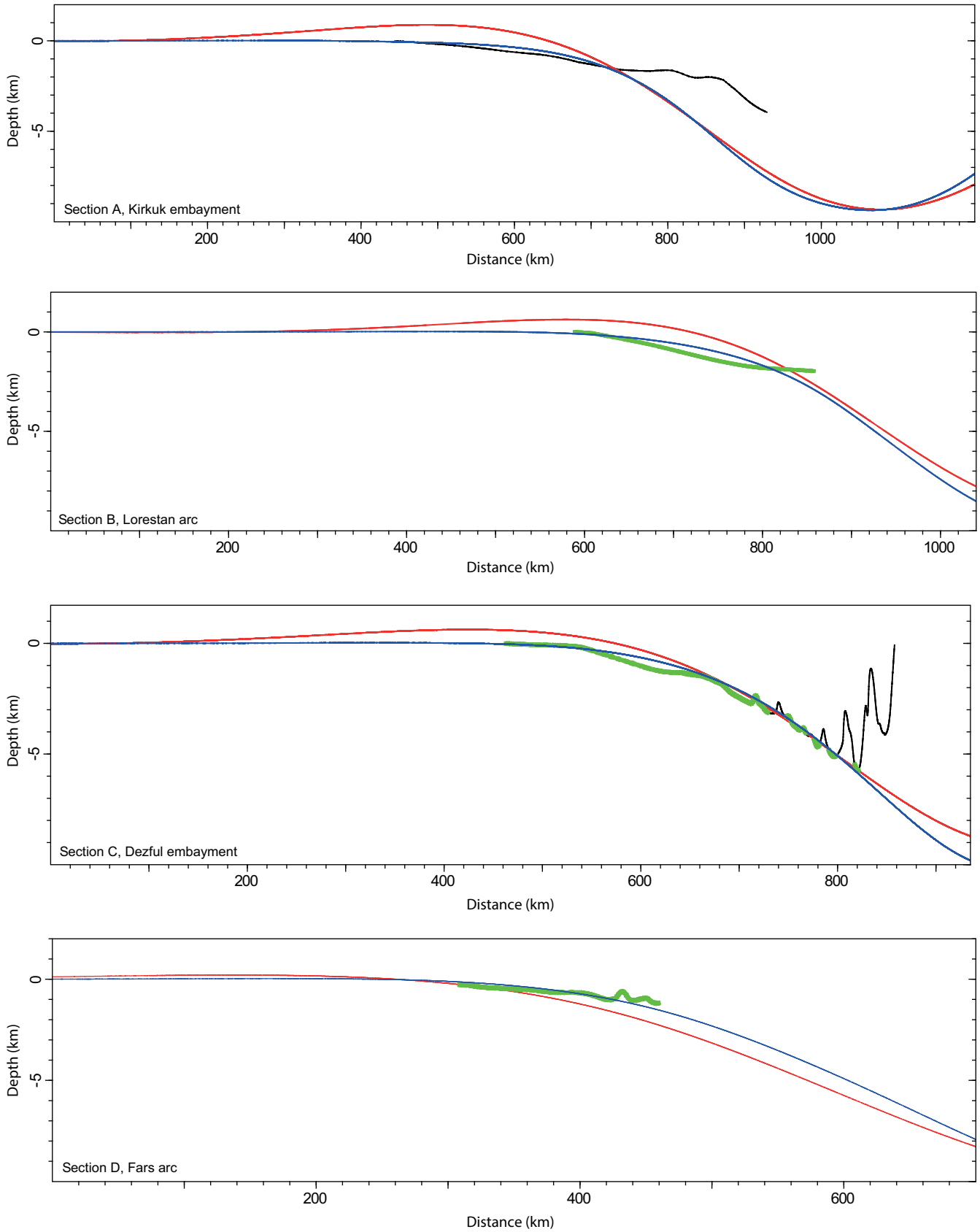

Figure 11. Observed and predicted foreland depths for best fitting Models 1 (red) and 2 (blue) along sections A, B, C and D. Black lines represent the depth to the Asmari Formation. Note that green overlaps black in sections B, C and D. The green outline highlights the portions within the area used to determine the best fitting model.

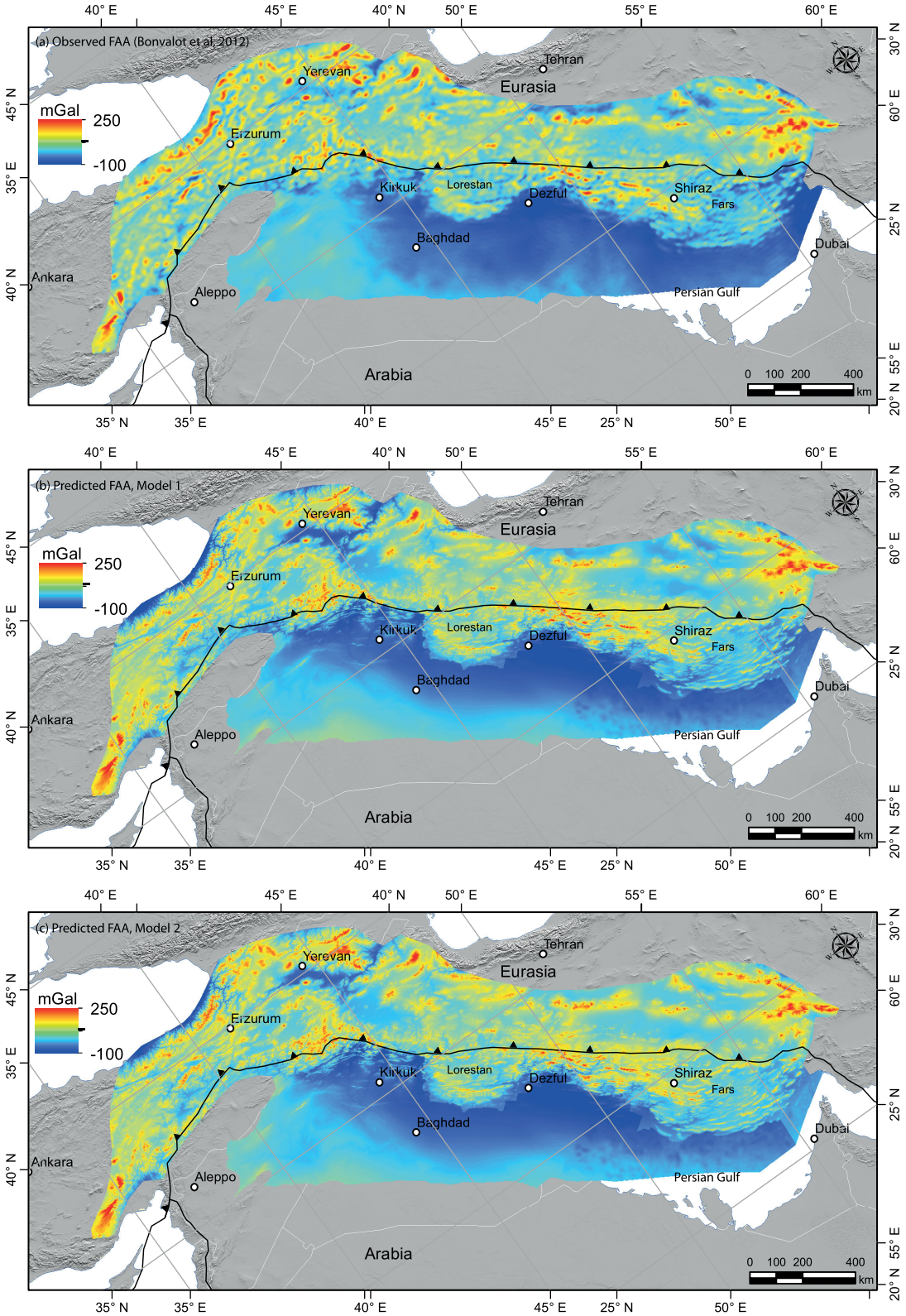

Figure 12. Observed FAA (Bonvalot *et al.* 2012) (a), and predicted FAA for Model 1 (b) and Model 2 (c). Residuals are shown in Supporting Information Figs S4 and S5.

and divide by the topography. For $\Delta\rho = 400$ kg m^{-3}, we obtain an average value of 5.3 which is very close to our estimate of the best fitting value of λ (Supporting Information Fig. S6). We conclude that, Model 2 does not imply any other source of loads than the Moho deflection and basin fill. This is why the best fitting Model 1 and Model 2 predict quite similar Moho geometries (Fig. 15).

The difference between Model 1 and Model 2 is larger in the western part of the model where the foreland basin is shallow. The

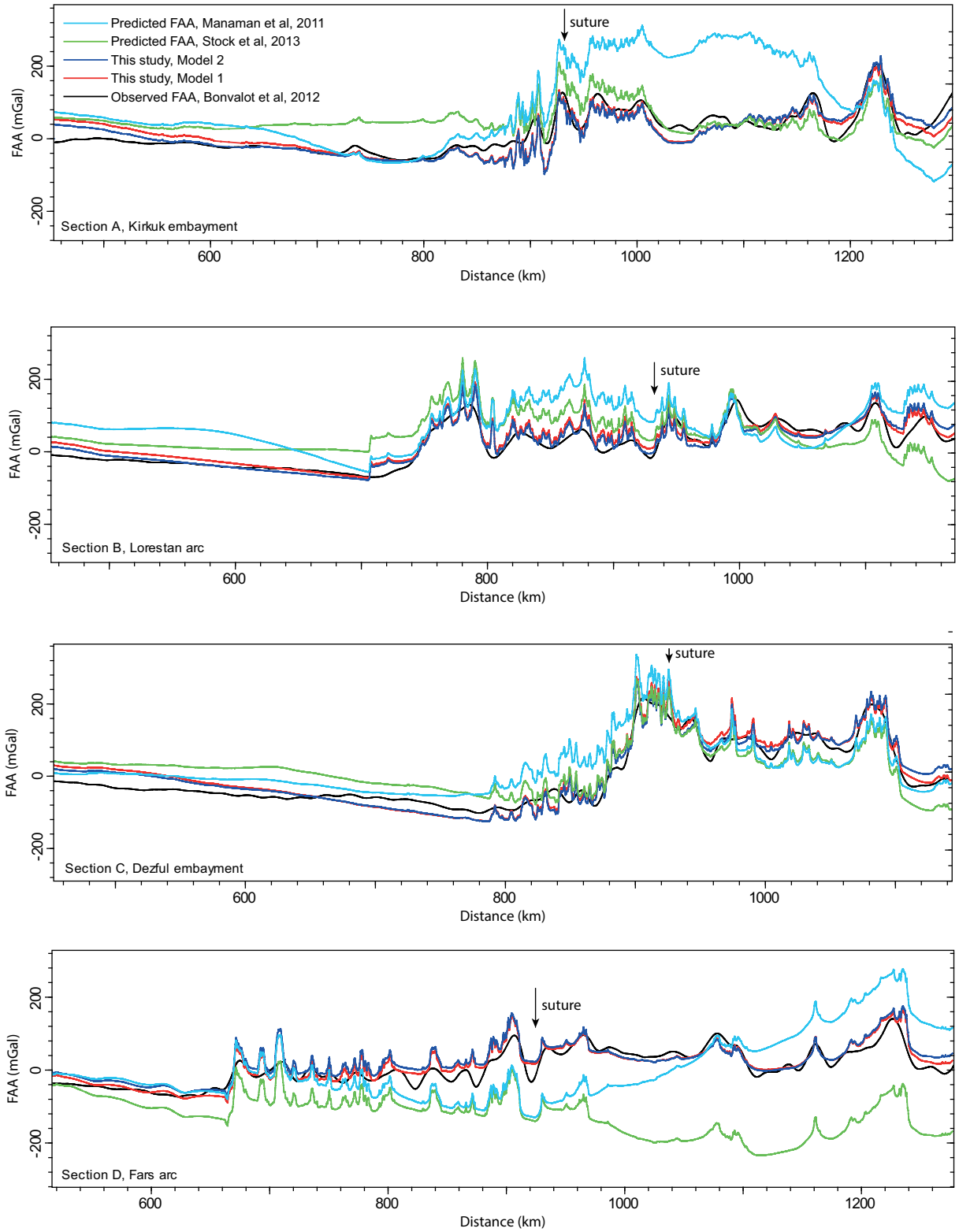

Figure 13. Comparison of observed FAA (black curve; Bonvalot *et al.* 2012), predicted FAA for Model 1 (red curve), and Model 2 (dark blue curve) along the sections A, B, C and D. We also show for comparison, the calculated FAA using the Moho depth derived from seismology by Stolk *et al*. (2013, green line) and Manaman *et al.* (2011, blue curve). Locations of sections are shown in Fig. 1.

difference is essentially due to the fact that Model 1 implicitly assumes a depressed Moho beneath the foreland (so it involved additional loading due to the thickened crust there) while the observed shallow basin depth implies only little loading from the sedimentary fill in Model 2. Model 1 reproduces arcuate shape of the foredeep with large depth (Fig. 10). By contrast Model 2 fails to predict the arcuate shape but yields a more reasonable basin depth. Fitting the observed geometry of the basin and the FAA in that area might require

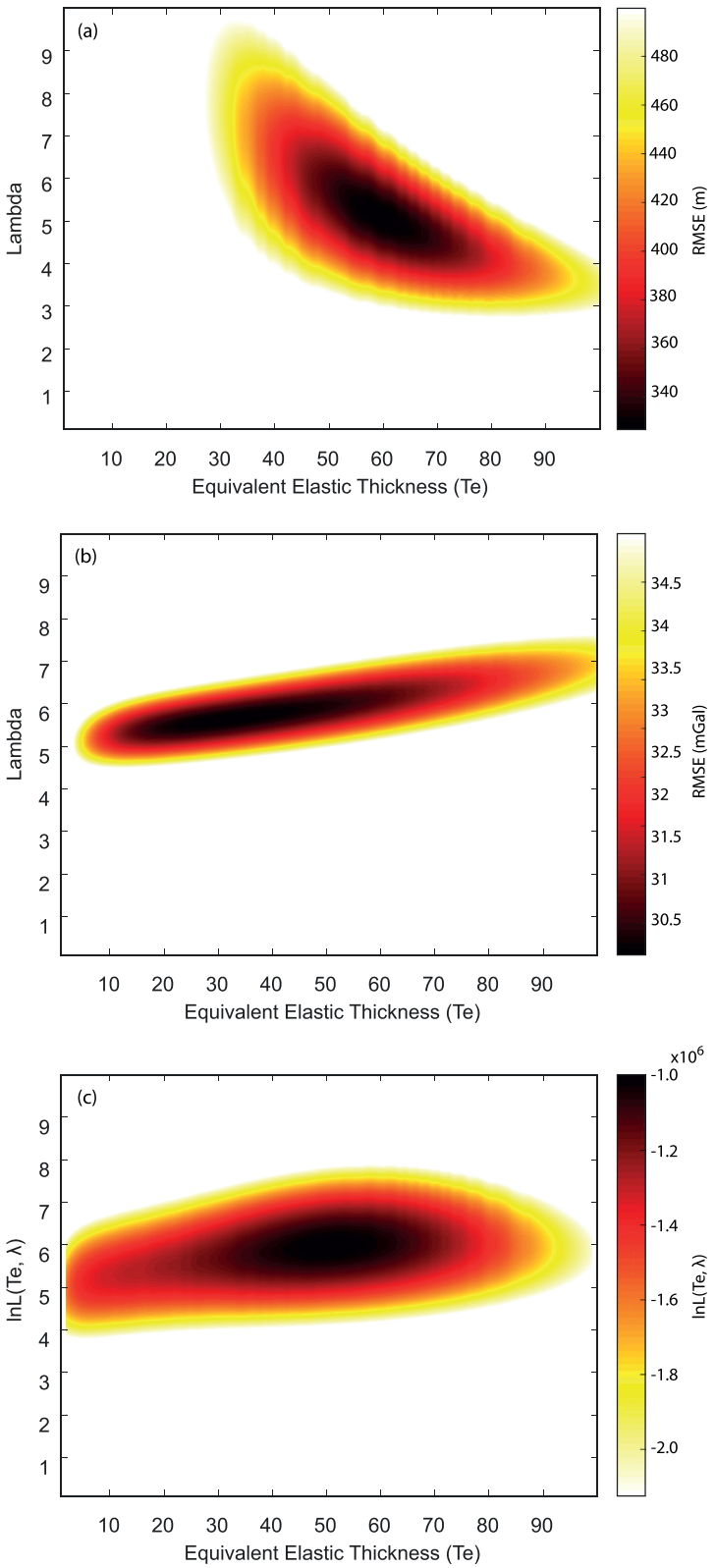

Figure 14. (a) RMSE between modelled and observed foreland depth as a function of T_e and λ for Model 2. (b) RMSE between observed and predicted FAA obtained for Model 2. (c) Logarithm of the likelihood of the joint pdf of the deflection and FAA data sets.

a different loads distribution than the ones presented here. Both Models 1 and 2 succeed at fitting simultaneously the foreland basin geometry and the FAA over the foreland and Zagros suggesting that our models account for the main factors flexing down the Arabian plate, that is, loading due to the topography of the Zagros, subsurface load by the thickened crustal root, and the sedimentary fill.

We conclude that, if we except the mismatch observed in the western sector of the study area (western Iraq and Syria), there is

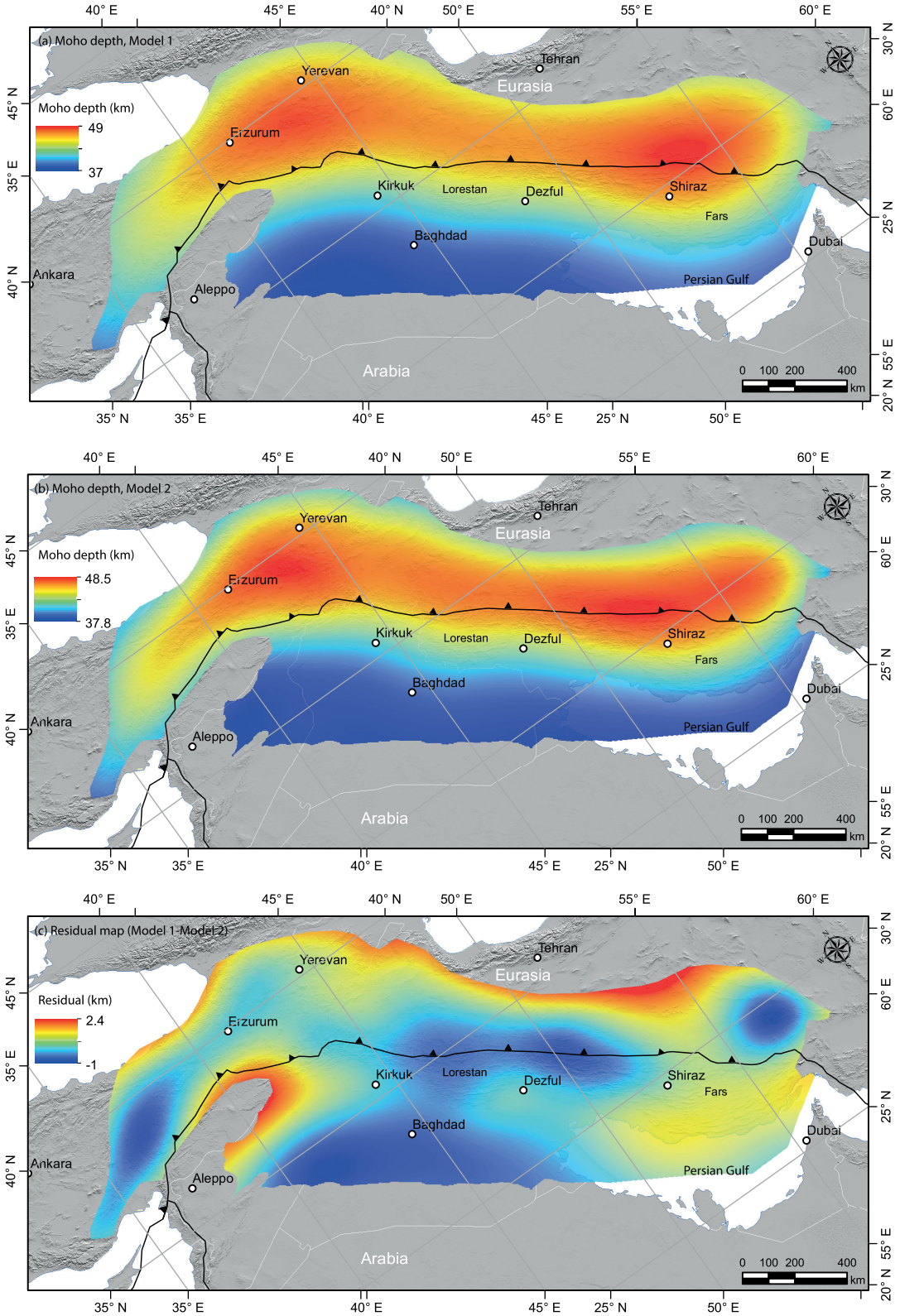

Figure 15. Moho depth predicted from Model 1 (a), Model 2 (b) and the difference between the two models, Model 1–Model 2 (c).

no need to invoke any significant additional loads than the static loads related to the topography, the crustal root and the sedimentary fill. We thus do not find any clear signature in the balance of forces applied to the lithosphere of dynamics effects possibly related to the dynamics of the subduction of the Arabian lithosphere, which could involve slab break-off or delamination of the thickened Eurasian lithosphere. In contrast, in the western section, the foreland is shallower than predicted by our models. It is possible that this sector would be influenced by mantle flow dynamics. This area could indeed be under the influence of the Afar mantle plume

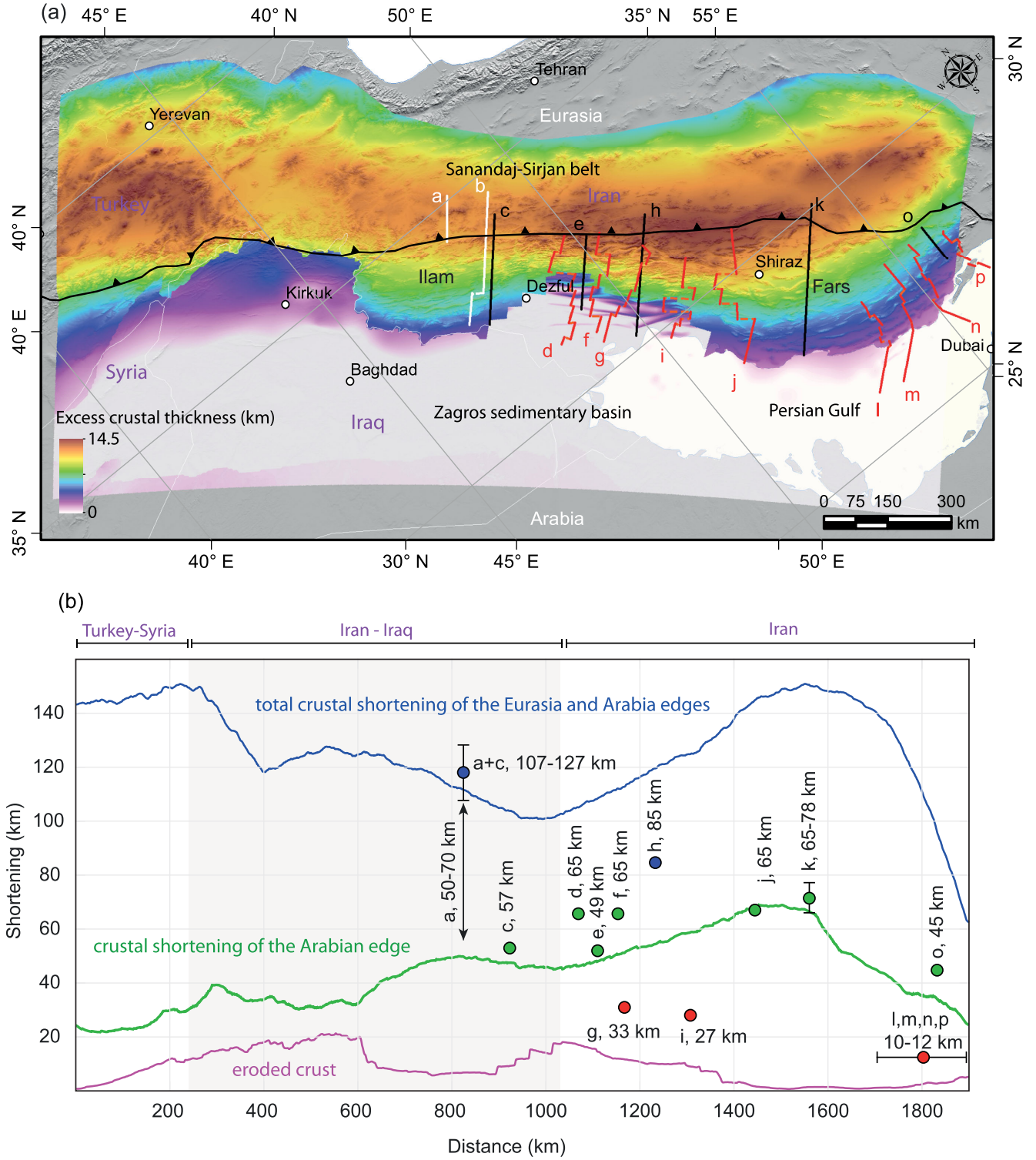

Figure 16. (a) Excess crustal thickness for Mode l2, assuming an initial crustal thickness of 38 km. (b) Longitudinal variation of crustal shortening determined from balancing N–S sections across the range. We assume plane strain deformation and conservation of volume. The blue line is the total shortening including the volume of the post-Asmari sediments deposited in the foreland. This calculation accounts for the density difference between the eroded bedrock and foreland sediments assuming that the volume of range topography eroded away is balanced by the volume of sediments deposited along N–S sections. The pink line shows the contribution of the eroded sediment to the total shortening. The Green line shows the shortening estimated from crustal thickening south of the Zagros suture zone. The plot also shows shortening estimates from the literature, which were determined from published structural sections. Locations of the sections are shown in panel (a). Section a (Agard *et al.* 2005), section b (Verges *et al.* 2011) represents 180 km of total crustal shortening, sections c, h and k (McQuarrie 2004; Mouthereau *et al.* 2007), sections d, f, g, i and j (Sherkati *et al.* 2006), section e (Blanc *et al.* 2003), sections l, m, n and p (Jahani *et al.* 2009) and section o (Molinaro *et al.* 2005). Symbols depend on whether the section represents shortening across nearly the whole wedge (Sanandaj-Sirjan belt and Zagros) which is shown with a blue circle, north of the suture with an arrow, and south of the suture with green circles. Red circles show shortening estimated along only a fraction of the distal portion of the Zagros wedge.

whose influence is recognized as far as the Aegean Sea (Chang *et al.* 2011; Faccenna *et al.* 2013; Jolivet *et al.* 2015). This feature causes warmer and weaker lithosphere in the eastern sector (Syria-Iraq) and may be a source of sublithospheric loads.

6.3 Moho geometry and implications for crustal shortening

Our flexural model predicts a Moho geometry that is in much better agreement with the observed FAA than seismology-based models of the Moho (Grad *et al.* 2009; Manaman *et al.* 2011; Mechie *et al.* 2013). These Moho geometries are roughly consistent on average but there are large local discrepancies (Fig. 6). Investigating the origins of the discrepancies between seismologically constrained and our Moho model is beyond the scope of this study. They could be related to interpretation of the original seismological observation or to the interpolation procedure. Given the good fit with the observed FAA, however, the Moho geometry derived from Model 2 provides an advanced guess of the crustal thickness variations in the Zagros.

This information can be used to estimate the post-collisional shortening based on a simple mass budget. To this aim, we assume that the thickness of the Arabian continental margin at the onset of the collision was homogeneous and that the topography was close to the sea-level. This assumption is justified for the northern edge of the Arabian platform given that the facies of the Asmari formation indicates a shallow marine environment with a depositional depth less than 250 m (Van Buchem *et al.* 2010). So we assume an initial crustal thickness was $T_c = 38$ km. An initial crustal thickness of 38 km is more questionable for the area north of the Noe-Tethyan suture on the southern flank of the Sanandaj-Sirjan metamorphic belt. The crust may have already been thickened due to the magmatic underplating related to the Neo-Tethyan subduction, and in the aftermath of accretion of the Cimmerian block to Eurasia (Hassanzadeh & Wernicke 2016). We assume conservation of mass at the scale of the orogen and its foreland (as defined by the box in Fig. 4). A fraction of the thickened crust has been eroded and is now stored in the post-Asmari fill of the foreland. For example, the volume between the topography and the Moho depth predicted by Model 2 is estimated as 7.36×10^7 km^3, where $\Delta\rho = 400$ kg m^{-3}. The volume of the post-Asmari fill of the foreland is estimated as 7.78×10^5 km^3. Given the lower density of the sediments in the foreland (Supporting Information Fig. S2) this corresponds to a volume of crust 5.69×10^5 km^3.

For simplicity, we ignore density changes resulting from the effect of metamorphic reactions on mineral volumes. Volume of the thickened crust and foreland sediments are assumed equal to the volume of the initial undeformed crust. We assume plane strain resulting from NS compression and NS transport of sediment.

With these assumptions, we first calculate the shortening across NS sections running across the Arabian margin, south of the suture, without taking the volume of the sediments into account (green line in Fig. 16). It should therefore be considered a minimum value of the shortening since the onset of the collision. We obtain a shortening of *ca.* 30 km in the western sector, which increases to 75 km in the Fars. The average value is 21 ± 9 km (mean and standard deviation) in Iraq and Syria and 45 ± 13 km in Iran.

We next proceed to include the volume of sediment and expand the calculation to the whole Zagros. The domain within which the post-collisional shortening is calculated is shown in Fig. 16a and the shortening values are plotted in Fig. 16b. The volume of sediment corresponds to the shortening of 9 ± 6 km on average. Section through the entire Zagros range (so including the Sanandaj-Sirjan metamorphic belt and Zagros fold-and-thrust belt) and taking the sediments into account yield a shortening which varies between 100 and 150 km (blue line in Fig. 16) with an average of 126 ± 18 km. The uncertainty associated with this estimate is not easy to constrain as it depends on the uncertainties on the foreland geometry, Moho depth and density distribution and their covariance. An attempt is made by calculating the shortening for a variety of models within the range of possible values of T_e and λ (we also varied the estimated volume of the foreland basin within 10 per cent). The obtained average range of the crustal shortening is *ca.* 125 ± 20 km where $\Delta\rho = 400 \pm 50$ kg m^{-3} (Table 1). We also estimate the shortening using the Moho geometry obtained with Model 1 which varies between 103 and 161 km for the same density variation. Finally, we also use the Moho model of Manaman *et al.* (2011) and got a value of 99 km for $\Delta\rho = 400$ kg m^{-3}. These calculations show that the shortening estimated based on our reconstructed Moho geometry is probably a rather robust quantity. Our estimates of crustal shortening are comparable to shortening values derived from palinspastic restoration of structural sections (Blanc *et al.* 2003; McQuarrie 2004; Agard *et al.* 2005; Molinaro *et al.* 2005; Sherkati *et al.* 2006; Mouthereau *et al.* 2007; Jahani *et al.* 2009; Verges *et al.* 2011). The agreement is remarkable given the different method and the crude assumptions made in our calculation (recall that we assumed the collision of two plates with the same constant initial crustal thickness, plain strain and volume conservation).

7 CONCLUSIONS

The post-collisional subsidence of the central and eastern sector of the Zagros foreland, determined by the depth to the Asmari formation, can be very well reproduced by a simple model of flexure of a thin elastic plate, which is in contrast with the need for extra subcrustal loads or dynamic stresses proposed in some previous studies. However, our model does not fit well with the actual depth of the western Zagros basin, in Iraq and Syria. Although it suggests that either variations in elastic thickness or a more complicated combination of subsurface loads, possibly caused by mantle dynamics, are needed. Our results highlight that the equivalent elastic thickness is $T_e = 50$ km beneath the foreland in Iran and probably decrease to *ca.* $T_e = 30$ km beneath the range. Compared to the observed gravity data, the calculated gravity data based upon our flexural model allows a better estimate of the Moho depth where the seismic investigation is absent or poor. Finally, our model of the Moho and foreland basin geometries implies a total shortening of 126 ± 18 km, due to post-collisional crustal shortening and ophiolite obduction, assuming that the whole area was initially at sea level and in isostatic equilibrium. Since this hypothesis is justified for the Arabian platform only, we obtain minimum shortening of 44 ± 13 km for deformed and eroded Arabian crust.

ACKNOWLEDGEMENTS

This study was partially supported by the Swiss National Science Foundation (grant P2GEP2–148801). Schlumberger provided a free academic license of the Petrel software. The quality of the paper was greatly improved by editorial guidance and constructive reviews from Associate Editor J.C. Afonso, and two anonymous reviewers. Sylvain Bonvalot, Dan McKenzie, James Jackson, Keith Priestley and Nicky White are thanked for useful discussions.

REFERENCES

Abdollahie Fard, I., Braathen, A., Mokhtari, M. & Alavi, S.A., 2006. Interaction of the Zagros Fold–Thrust Belt and the Arabian-type, deep-seated folds in the Abadan Plain and the Dezful Embayment, °SW Iran, *Pet. Geosci.,* **12,** 347–362.

Agard, P., Omrani, J., Jolivet, L. & Mouthereau, F., 2005. Convergence history across Zagros (Iran): constraints from collisional and earlier deformation, *Int. J. Earth Sci.,* **94,** 401–419.

Agard, P. *et al.*, 2011. Zagros orogeny: a subduction-dominated process, *Geol. Mag.,* **148,** 692–725.

Alavi, M., 2004. Regional stratigraphy of the Zagros fold-thrust belt of Iran and its proforeland evolution, *Am. J. Sci.,* **304,** 1–20.

Baban, E.N., Aziz, B.Q. & Aziz, N.H., 2014. Study of subsurface structures using seismic reflection data for Kalar–Khanaqin area/Kurdistan region, Iraq, *Arab. J. Geosci.,* **7,** 2279–2291.

Balmino, G., Vales, N., Bonvalot, S. & Briais, A., 2012. Spherical harmonic modelling to ultra-high degree of Bouguer and isostatic anomalies, *J. Geod.,* **86,** 499–520.

Beaumont, C., 1981. Foreland basins, *Geophys. J. R. astr. Soc.,* **65,** 291–329.

Berberian, M. & King, G.C.P., 1981. Towards a paleogeography and tectonic evolution of Iran, *Can. J. Earth Sci.,* **18,** 210–265.

Beydoun, Z.R., Clarke, M.W.H. & Stoneley, R., 1992. Petroleum in the Zagros Basin: a late tertiary foreland basin overprinted onto the outer edge of a vast hydrocarbon-rich paleozoic-mesozoic passive-margin shelf, in *Foreland Basins and Fold Belts*, vol. 55, pp. 309–339, eds McQueen, R.W. & Leckie, D.A., The American Association of Petroleum Geologists.

Bird, P., 1978. Finite element modeling of lithosphere deformation: the Zagros collision orogeny, *Tectonophysics,* **50,** 307–336.

Blanc, E.J.P., Allen, M.B., Inger, S. & Hassani, H., 2003. Structural styles in the Zagros Simple Folded Zone, Iran, *J. Geol. Soc.,* **160,** 401–412.

Bonvalot, S. *et al.*, 2012. *World Gravity Map, 1:50000000 Map,* BGI-CGMW-CNES-IRD.

Brew, G., Litak, R., Barazangi, M., Sawaf, T. & Zaza, T., 1999. Tectonic evolution of northeast Syria: regional implications and hydrocarbon prospects, *GeoArabia,* **4,** 289–318.

Brotchie, J. & Silvester, R., 1969. On crustal flexure, *J. geophys. Res.,* **74,** 5240–5252.

Burgmann, R. & Dresen, G., 2008. Rheology of the lower crust and upper mantle: Evidence from rock mechanics, geodesy, and field observations, *Annu. Rev. Earth Planet. Sci.,* **36,** 531–567.

Burov, E.B., 2011. Rheology and strength of the lithosphere, *Mar. Pet. Geol.,* **28,** 1402–1443.

Burov, E.B. & Diament, M., 1992. Flexure of the continental lithosphere with multilayered rheology, *Geophys. J. Int.,* **109,** 449–468.

Burov, E.B. & Diament, M., 1995. The effective elastic thickness (Te) of continental lithosphere: what does it really mean?, *J. geophys. Res.,* **100,** 3905–3927.

Cattin, R., Martelet, G., Henry, P., Avouac, J.P., Diament, M. & Shakya, T.R., 2001. Gravity anomalies, crustal structure and thermo-mechanical support of the Himalaya of Central Nepal, *Geophys. J. Int.,* **147,** 381–392.

Chang, S.-J., Merino, M., Van der Lee, S., Stein, S. & Stein, C.A., 2011. Mantle flow beneath Arabia offset from the opening Red Sea, *Geophys. Res. Lett.,* **38,** L04301, doi:10.1029/2010GL045852.

Chen, B., Kaban, M.K., El Khrepy, S. & Al-Arifi, N., 2015. Effective elastic thickness of the Arabian plate: weak shield versus strong platform, *Geophys. Res. Lett.,* **42,** 3298–3304.

DeCelles, P.G., 2011. Foreland basin systems revisited: variations in response to tectonic settings, in *Tectonics of Sedimentary Basins: Recent Advances*, pp. 405–426, eds Busby, C. & Azor, A., John Wiley & Sons.

DeCelles, P.G. & Giles, K.A., 1996. Foreland basin systems, *Basin Res.,* **8,** 105–123.

Emami, H., 2008. Foreland propagation folding and structure of the mountain front flexture in the Posht-e-kuh are (NW Zagros, Iran), *PhD thesis,* Universitat de Barcelona, Barcelona.

Emery, K.O., 1956. Sediments and water of Persian Gulf, *AAPG Bull.,* **40,** 2354–2383.

Faccenna, C., Becker, T.W., Jolivet, L. & Keskin, M., 2013. Mantle convection in the Middle East: reconciling afar upwelling, Arabia indentation and Aegean trench rollback, *Earth planet. Sci. Lett.,* **375,** 254–269.

Falcon, N.L., 1974. Southern Iran: Zagros Mountains, *Geol. Soc., London, Spec. Publ.,* **4,** 199–211.

Farr, T.G. *et al.*, 2007. The shuttle radar topography mission, *Rev. Geophys.,* **45,** RG2004, doi:10.1029/2005RG000183.

Garcia-Castellanos, D., 2002. Interplay between lithospheric flexure and river transport in foreland basins, *Basin Res.,* **14,** 89–104.

Gavillot, Y., Axen, G.J., Stockli, D.F., Horton, B.K. & Fakhari, M.D., 2010. Timing of thrust activity in the High Zagros fold-thrust belt, Iran, from (U-Th)/He thermochronometry, *Tectonics,* **29,** TC4025, doi:10.1029/2009TC002484.

Grad, M., Tiira, T. & Group, E.W., 2009. The Moho depth map of the European Plate, *Geophys. J. Int.,* **176,** 279–292.

Hargrove, U., Stern, R., Kimura, J.-I., Manton, W. & Johnson, P., 2006. How juvenile is the Arabian–Nubian shield? Evidence from Nd isotopes and pre-Neoproterozoic inherited zircon in the Bi'r Umq suture zone, Saudi Arabia, *Earth planet. Sci. Lett.,* **252,** 308–326.

Hassanzadeh, J. & Wernicke, B.P., 2016. The Neotethyan Sanandaj-Sirjan zone of Iran as an archetype for passive margin-arc transitions, *Tectonics,* **35,** 586–621.

Hatzfeld, D. & Molnar, P., 2010. Comparisons of the kinematics and deep structures of the Zagros and Himalaya and of the Iranian and Tibetan plateaus and geodynamic implications, *Rev. Geophys.,* **48,** RG2005, doi:10.1029/2009RG000304.

Hetenyi, G., Cattin, R., Vergne, J. & Nabelek, J.L., 2006. The effective elastic thickness of the India Plate from receiver function imaging, gravity anomalies and thermomechanical modelling, *Geophys. J. Int.,* **167,** 1106–1118.

Hetenyi, G., Cattin, R., Brunet, F., Bollinger, L., Vergne, J., Nabelek, J. & Diament, M., 2007. Density distribution of the India plate beneath the Tibetan plateau: Geophysical and petrological constraints on the kinetics of lower-crustal eclogitization, *Earth planet. Sci. Lett.,* **264,** 226–244.

Heydari, E., 2008. Tectonics versus eustatic control on supersequences of the Zagros Mountains of Iran, *Tectonophysics,* **451,** 56–70.

Homke, S., Vergés, J., Garcés, M., Emami, H. & Karpuz, R., 2004. Magnetostratigraphy of Miocene–Pliocene Zagros foreland deposits in the front of the Push-e Kush Arc (Lurestan Province, Iran), *Earth planet. Sci. Lett.,* **225,** 397–410.

Jackson, J., McKenzie, D., Priestley, K. & Emmerson, B., 2008. New views on the structure and rheology of the lithosphere, *J. Geol. Soc.,* **165,** 453–465.

Jackson, J.A., 1980. Reactivation of basement faults and crustal shortening in orogenic belts, *Nature*, **283,** 343–346.

Jahani, S., Callot, J.-P., Letouzey, J. & Frizon de Lamotte, D., 2009. The eastern termination of the Zagros Fold-and-Thrust Belt, Iran: structures, evolution, and relationships between salt plugs, folding, and faulting, *Tectonics,* **28,** TC6004, doi:10.1029/2008TC002418.

Jassim, S.Z. & Goff, J.C., 2006. *Geology of Iraq,* Geological Society of London.

Jimenez-Munt, I., Fernandez, M., Saura, E., Verges, J. & Garcia-Castellanos, D., 2012. 3-D lithospheric structure and regional/residual Bouguer anomalies in the Arabia–Eurasia collision (Iran), *Geophys. J. Int.,* **190,** 1311–1324.

Jolivet, L. *et al.*, 2015. The geological signature of a slab tear below the Aegean, *Tectonophysics,* **659,** 166–182.

Kaban, M.K., El Khrepy, S. & Al-Arifi, N., 2016. Isostatic model and isostatic gravity anomalies of the Arabian Plate and surroundings, *Pure appl. Geophys.,* **173,** 1211–1221.

Karner, G.D. & Watts, A.B., 1983. Gravity anomalies and flexure of the lithosphere at mountain ranges, *J. geophys. Res.,* **88,** 10 449–10 477.

Kent, N., 2010. Structures of the Kirkuk Embayment, northern Iraq: foreland structures or Zagros Fold Belt structures?, *GeoArabia,* **15,** 147–188.

Khadivi, S. *et al.*, 2010. Magnetochronology of synorogenic Miocene foreland sediments in the Fars arc of the Zagros Folded Belt (SW Iran), *Basin Res.,* **22,** 918–932.

Khadivi, S., Mouthereau, F., Barbarand, J., Adatte, T. & Lacombe, O., 2012. Constraints on palaeodrainage evolution induced by uplift and exhumation on the southern flank of the Zagros-Iranian Plateau, *J. Geol. Soc.,* **169,** 83–97.

Kirby, J. & Swain, C., 2009. A reassessment of spectral T_e estimation in continental interiors: the case of North America, *J. geophys. Res.,* **114,** B08401, doi:10.1029/2009JB006356.

Koop, W.J., Stoneley, R., Ridd, M.F., Murphy, R.W., Osmaston, M.F. & Kholief, M.M., 1982. Subsidence history of the Middle East Zagros Basin, Permian to recent [and discussion], *Phil. Trans. R. Soc. A,* **305,** 149–168.

Lyon-Caen, H. & Molnar, P., 1983. Constraints on the structure of the Himalaya from an analysis of gravity anomalies and a flexural model of the lithosphere, *J. geophys. Res.,* **88,** 8171–8191.

Manaman, N.S., Shomali, H. & Koyi, H., 2011. New constraints on upper-mantle S-velocity structure and crustal thickness of the Iranian plateau using partitioned waveform inversion, *Geophys. J. Int.,* **184,** 247–267.

McKenzie, D., 2003. Estimating T_e in the presence of internal loads, *J. geophys. Res.,* **108**(B9) 2438, doi:10.1029/2002JB001766.

McKenzie, D. & Fairhead, D., 1997. Estimates of the effective elastic thickness of the continental lithosphere from Bouguer and free air gravity anomalies, *J geophys. Res.,* **102,** 27 523–27 552.

McQuarrie, N., 2004. Crustal scale geometry of the Zagros fold-thrust belt, Iran, *J. Struct. Geol.,* **26,** 519–535.

Mechie, J., Ben-Avraham, Z., Weber, M., Götze, H.-J., Koulakov, I., Mohsen, A. & Stiller, M., 2013. The distribution of Moho depths beneath the Arabian plate and margins, *Tectonophysics,* **609,** 234–249.

Molinaro, M., Leturmy, P., Guezou, J.C., Frizon de Lamotte, D. & Eshraghi, S.A., 2005. The structure and kinematics of the southeastern Zagros fold-thrust belt, Iran: from thin-skinned to thick-skinned tectonics, *Tectonics,* **24,** TC3007, doi:10.1029/2004TC001633.

Molnar, P. & Lyon-Caen, H., 1988. Some simple physical aspects of the support, structure, and evolution of mountain belts, *Geol. Soc. Am. Spec., Pap.,* **218,** 179–208.

Mooney, W., 2010. 11 Crust and Lithospheric Structure–Global Crustal Structure, in *Seismology and Structure of the Earth: Treatise on Geophysics*, pp. 361–417, eds Romanowicz, B. & Dziewonski, A., Elsevier.

Motiei, H., 1993. *Stratigraphy of Zagros,* Geological Survey of Iran.

Mouthereau, F., Tensi, J., Bellahsen, N., Lacombe, O., Boisgrollier, T.D. & Kargar, S., 2007. Tertiary sequence of deformation in a thin-skinned/thick-skinned collision belt: The Zagros Folded Belt (Fars, Iran), *Tectonics,* **26,** TC5006, doi:10.1029/2007TC002098.

Mouthereau, F., Lacombe, O. & Verges, J., 2012. Building the Zagros collisional orogen: timing, strain distribution and the dynamics of Arabia/Eurasia plate convergence, *Tectonophysics,* **532,** 27–60.

Nissen, E., Tatar, M., Jackson, J.A. & Allen, M.B., 2011. New views on earthquake faulting in the Zagros fold-and-thrust belt of Iran, *Geophys. J. Int.,* **186,** 928–944.

Paul, A., Hatzfeld, D., Kaviani, A., Tatar, M. & Péquegnat, C., 2010. Seismic imaging of the lithospheric structure of the Zagros mountain belt (Iran), *Geol. Soc., London, Spec. Publ.,* **330,** 5–18.

Pérez-Gussinyé, M. & Watts, A., 2005. The long-term strength of Europe and its implications for plate-forming processes, *Nature,* **436,** 381–384.

Pérez-Gussinyé, M., Lowry, A.R., Watts, A.B. & Velicogna, I., 2004. On the recovery of effective elastic thickness using spectral methods: examples from synthetic data and from the Fennoscandian Shield, *J. geophys. Res.*, **109,** B10409, doi:10.1029/2003JB002788.

Perotti, C., Bertozzi, G., Feltre, L., Rahimi, M., Rinaldi, M. & Carruba, S., 2011. *The Qatar-South Fars Arch Development (Arabian Platform, Persian Gulf): Insights from Seismic Interpretation and Analogue Modelling,* INTECH Open Access Publisher.

Pirouz, M., 2013. The geometry and sedimentary record of tectonics in the Neogene Zagros foreland basin, *PhD thesis,* University of Geneva, Geneva.

Pirouz, M., Simpson, G., Bahroudi, A. & Azhdari, A., 2011. Neogene Sediments and Modern Depositional Environments of the Zagros Foreland Basin System, *Geol. Mag.,* **148,** 838–853.

Pirouz, M., Avouac, J., Simpson, G., Hassanzadeh, J., Herman, F. & Sternai, P., 2014. Orogen-parallel variation in flexure of the Arabian Plate beneath the Zagros mountains, in *AGU Fall Meeting,* Abstract #T43C-4751.

Pirouz, M., Simpson, G. & Chiaradia, M., 2015. Constraint on foreland basin migration in the Zagros mountain belt using Sr isotope stratigraphy, *Basin Res.,* **27,** 714–728.

Pirouz, M., Simpson, G., Castelltort, S., Gorin, G. & Bahroudi, A., 2016. Controls on the sequence stratigraphic architecture of the Neogene Zagros foreland basin, *Geol. Soc. Am. Spec. Pap.,* **525,** SPE525-512. doi:10.1130/2016.2525(12).

Priestley, K., McKenzie, D., Barron, J., Tatar, M. & Debayle, E., 2012. The Zagros core: deformation of the continental lithospheric mantle, *Geochem. Geophys. Geosyst.,* **13,** Q11014, doi:10.1029/2012GC004435.

Purser, B.H. & Seibold, E., 1973. The principal environmental factors influencing Holocene sedimentation and diagenesis in the Persian Gulf, in *The Persian Gulf Holocene Carbonate Sedimentation and Diagenesis in a Shallow Epicontinental Sea,* pp. 1–9, ed. Purser, B.H., Springer-Verlag.

Reilinger, R. & McClusky, S., 2011. Nubia-Arabia-Eurasia plate motions and the dynamics of Mediterranean and Middle East tectonics, *Geophys. J. Int.,* **186,** 971–979.

Royden, L., 1988. Flexural behavior of the continental lithosphere in Italy—constraints imposed by gravity and deflection data, *J. geophys. Res.,* **93,** 7747–7766.

Royden, L.H., 1993. The steady state thermal structure of eroding orogenic belts and accretionary prisms, *J. geophys. Res.,* **98,** 4487–4507.

Saura, E., Garcia-Castellanos, D., Casciello, E., Parravano, V., Urruela, A. & Verges, J., 2015. Modeling the flexural evolution of the Amiran and Mesopotamian foreland basins of NW Zagros (Iran-Iraq), *Tectonics,* **34,** 377–395.

Sepehr, M., Cosgrove, J. & Moieni, M., 2006. The impact of cover rock rheology on the style of folding in the Zagros fold-thrust belt, *Tectonophysics,* **427,** 265–281.

Sherkati, S., Letouzey, J. & Frizon de Lamotte, D., 2006. Central Zagros fold-thrust belt (Iran): new insights from seismic data, field observation, and sandbox modeling, *Tectonics,* **25,** TC4007, doi:10.1029/2004TC001766.

Snyder, D.B. & Barazangi, M., 1986. Deep crustal structure and flexure of the Arabian Plate Beneath the Zagros collisional mountain belt as inferred from gravity observations, *Tectonics,* **5,** 361–373.

Soleimani, B., 2010. Reactivation of deep seated folds in Northwest Persian Gulf, *PhD thesis*, Barcelona, Grup de Geodinàmica i Anàlisi de Conques.

Stern, R. & Manton, W., 1987. Age of Feiran basement rocks, Sinai: implications for late Precambrian crustal evolution in the northern Arabian–Nubian Shield, *J. Geol. Soc.,* **144,** 569–575.

Stocklin, J., 1968. Structural history and tectonics of Iran: a review, *AAPG Bull.,* **52,** 1229–1258.

Stolk, W., Kaban, M., Beekman, F., Tesauro, M., Mooney, W.D. & Cloetingh, S., 2013. High resolution regional crustal models from irregularly distributed data: application to Asia and adjacent areas, *Tectonophysics,* **602,** 55–68.

Talebian, M. & Jackson, J., 2004. A reappraisal of earthquake focal mechanisms and active shortening in the Zagros mountains of Iran, *Geophys. J. Int.,* **156,** 506–526.

Tesauro, M., Audet, P., Kaban, M.K., Bürgmann, R. & Cloetingh, S., 2012. The effective elastic thickness of the continental lithosphere: comparison between rheological and inverse approaches, *Geochem. Geophys. Geosyst.,* **13,** Q09001, doi:10.1029/2012GC004162.

Tesauro, M., Kaban, M.K. & Cloetingh, S.A., 2013. Global model for the lithospheric strength and effective elastic thickness, *Tectonophysics,* **602,** 78–86.

Tunini, L., Jiménez-Munt, I., Fernandez, M., Vergés, J. & Villaseñor, A., 2015. Lithospheric mantle heterogeneities beneath the Zagros Mountains and the Iranian Plateau: a petrological-geophysical study, *Geophys. J. Int.,* **200,** 596–614.

Van Buchem, F.S.P. *et al.*, 2010. Regional stratigraphic architecture and reservoir types of the Oligo-Miocene deposits in the Dezful Embayment

(Asmari and Pabdeh Formations) SW Iran, *Geol. Soc., London, Spec. Publ.,* **329,** 219–263.

Verges, J., Saura, E., Casciello, E., Fernandez, M., Villasenor, A., Jimenez-Munt, I. & Garcia-Castellanos, D., 2011. Crustal-scale cross-sections across the NW Zagros belt: implications for the Arabian margin reconstruction, *Geol. Mag.,* **148,** 739–761.

Watts, A.B., 2001. *Isostasy and Flexure of the Lithosphere,* Cambridge Univ. Press.

Watts, A.B. & Burov, E.B., 2003. Lithospheric strength and its relationship to the elastic and seismogenic layer thickness, *Earth. Planet. Sci. Lett.,* **213,** 113–131.

Wienecke, S., Braitenberg, C. & Götze, H.-J., 2007. A new analytical solution estimating the flexural rigidity in the Central Andes, *Geophys. J. Int.,* **169,** 789–794.

Zamani, A., Samiee, J. & Kirby, J.F., 2014. The effective elastic thickness of the lithosphere in the collision zone between Arabia and Eurasia in Iran, *J. Geodyn.,* **81,** 30–40.

SUPPORTING INFORMATION

Supplementary data are available at *GJI* online.

Figure S1. Root mean square residual (RMSE) between observed and predicted FAA using the seismologically constrained Moho model of Manaman *et al*. (2011) and WGM12 surface Free Air Anomaly (Bonvalot *et al.* 2012). The model prediction assumes a constant crust density of 2670 kg m^{-3}. The minimum RMSE corresponds to 3060 kg m^{-3} (i.e. $\Delta\rho = 390$ kg m^{-3}) of mantle density and $T_c = 37.8$ km in the eastern sector.

Figure S2. Density distribution versus depth in the Zagros foreland basin. Red curve represents measured density in the borehole and the green curve is calculated density curve using the sonic log (DT) from the same borehole. The well is located in the Dezful embayment. See green circle in Fig. 3 for approximate location. We converted sonic log to density from the equation obtained from least-squares regression to the portion of the data set where the two measurements are available. The black coloured curve corresponds to degree 2 polynomial function that best fits the depth distribution of density.

Figure S3. Simulated plate deflection due to the weight of the basin deposits applied to an elastic thin plate overlying an inviscid fluid with density $\rho_m = 3070$ kg m^{-3}. (a) Measured post-collisional deflection determined from the depth to the Asmari formation. This information is combined with the depth distribution of density, Fig. S2, to determine the basin load distribution. (b–d) Model prediction using an equivalent elastic thickness (T_e) of 5, 20 and 50 km, respectively

Figure S4. Residuals between observed FAA (Bonvalot *et al.* 2012) and predicted FAA from Model 1 (a) and Model 2 (b) and seismic Moho depth (c).

Figure S5. Residuals between observed Bouguer anomaly (Bonvalot *et al.* 2012) and predicted Bouguer anomaly from Model 1 (a) and Model 2 (b).

Figure S6. The crustal thickness of Model 2 divided by the topography in map view (a) and histogram (b) for $\Delta\rho = 400$ kg m^{-3}. The mean value is 5.3 and standard deviation is 1.8. The obtained mean value is comparable to the estimated λ in the flexural Model 2.

Please note: Oxford University Press is not responsible for the content or functionality of any supporting materials supplied by the authors. Any queries (other than missing material) should be directed to the corresponding author for the paper.